BRE large compartment fire tests – characterising post-flashover fires for model validation

S. Welch*, A. Jowsey, S. Deeny, R. Morgan, J.L. Torero

School of Engineering and Electronics, The University of Edinburgh, Edinburgh, EH9 3JL, UK

Abstract

Reliable and comprehensive measurement data from large-scale fire tests is needed for validation of computer fire models, but is subject to various uncertainties, including radiation errors in temperature measurement. Here, a simple method for post-processing thermocouple data is demonstrated, within the scope of a series of large-scale fire tests, in order to establish a well characterised dataset of physical parameter values which can be used with confidence in model validation. Sensitivity analyses reveal the relationship of the correction uncertainty to the assumed optical properties and the thermocouple distribution. The analysis also facilitates the generation of maps of an equivalent radiative flux within the fire compartment, a quantity which usefully characterises the thermal exposures of structural components. Large spatial and temporal variations are found, with regions of most severe exposures not being collocated with the peak gas temperatures; this picture is at variance with the assumption of uniform heating conditions often adopted for post-flashover fires.

Keywords: Post-flashover fire, Model validation, CFD model, Thermocouple temperature, Radiative flux, Natural fire safety concept

* Corresponding author. Tel.: + 44-131-6505734; fax: + 44-131-6506781

Nomenclature

A	-	area [m^2]
b	-	thermal absorptivity, $\sqrt{k\rho c_p}$ [$J/m^2/s^{1/2}/K$]
$C_{1,2}$	-	viscosity model constants [$kg/m/s/K^{0.5}$, K]
c_p	-	specific heat capacity [J/kg/K]
d	-	diameter [m]
h	-	heat transfer coefficient [$W/m^2/K$]
h_{eq}	-	weighted average of window heights on all walls [m]
I	-	radiative intensity [W/sr]
k	-	thermal conductivity [W/m/K]
K_t	-	velocity probe calibration factor [-]
L	-	path length [m]
L_i	-	total distance from origin thermocouple, $i=1$, *to* thermocouple TC_i [m]
ΔL_i	-	path length associated with thermocouple TCi, in direction of origin [m]
Nu	-	Nusselt number (hd/k) (dimensionless heat transfer coefficient) [-]
O	-	opening factor ($A_v\sqrt{h_{eq}}/A_t$) [$m^{1/2}$]
p	-	pressure [N/m^2]
Pr	-	Prandtl number ($\mu c_p/k$) (kinematic viscosity/thermal diffusivity) [-]
$\dot{q}''$	-	heat flux [W/m^2]
r	-	radius [m]; relaxation factor [-]
T	-	temperature [K]
t	-	time [s]
U	-	velocity [m/s]
V	-	volume [m^3]
W	-	weighting factor [-]
ε	-	emissivity [-]
κ	-	extinction coefficient [m^{-1}]
μ	-	coefficient of viscosity [kg/m/s]
ρ	-	density [kg/m^3]
σ	-	Stefan-Boltzmann constant [$5.67\text{x}10^{-8}$ $W/m^2/K^4$]

Subscripts/superscripts

a	-	ambient
$conv$	-	convective
gas	-	gas
i	-	thermocouple i
inc	-	incident
net	-	net
s	-	surroundings
rad	-	radiative
t	-	total surface, i.e. walls, ceiling and floor, including openings
tot	-	total, i.e. convective plus radiative
TC	-	thermocouple
v	-	vertical openings on all walls

E-mail address: s.welch@ed.ac.uk (S. Welch).

1. Introduction

The availability of reliable and comprehensive measurement data from large-scale fire tests is essential for the ongoing validation of computational simulation methodologies for fire, and computational fluid dynamic (CFD) models in particular [1-3]. The validation exercise is complicated by various uncertainties both in the input parameters for the models and the measured fire parameters themselves [1-3]. The former include, for example, determining an accurate heat release rate for the fire and relevant temperature-dependent material properties, whilst the latter typically involves measurement errors in the values of temperature, velocity, heat flux and species data. Some of these uncertainties derive simply from the instrument tolerances, but the errors in temperature measurement are compromised by a more systematic uncertainty known as the "radiation error" [3-5]. This is named after the fact that remote radiation may influence the thermocouple measurement, such that the reported temperatures may differ greatly from the local gas temperature, particularly in "lower layer" regions. These effects are well known [1-7] and are not "errors" *per se*, merely characteristics of the measurement device, but clearly need careful consideration when the experimental data are used in the validation of model predictions expressed in terms of gas temperatures. There is also some knock--on effect of temperature uncertainty on other measurements, including heat fluxes and gas velocities, where, respectively, the local gas temperature appears directly in the convective term and is referenced in the conversion from the measured pressure difference [8,1].

The hypothesis made here is that given the availability of a sufficient number of measurement points it is theoretically possible to compute an estimate of the true gas

temperatures at each location by post-processing the thermocouple temperature data taking account of the expected interactions in the thermal flowfield. The corrected temperatures can then be used in determining the true gas velocities and may be cross-checked by assessing consistency with measured heat fluxes. However, recognising the theoretical interrelationship of each thermocouple temperature with every other, and second-order couplings such as the interrelationships between temperature, optical properties and velocity, it is apparent that the problem is mathematically complex, requiring a numerical solution. The main content of this paper is the description and demonstration of a simple method for performing this post-processing, within the scope of a series of large-scale fire tests. The ultimate aim is to establish a self-consistent and reliable dataset of physical parameter values which can be used with confidence in model validation. This analysis also facilitates sensitivity analyses of the effects of uncertain parameters, such as the optical properties of the combustion gases, and the generation of radiative flux maps, which can provide a valuable insight into the spatial and temporal variability of the thermal exposures within the fire compartment.

The experimental programme was undertaken within the scope of the Natural Fire Safety Concept 2 (NFSC2) series of fire tests at BRE Cardington in 1999-2000, sponsored by the European Coal and Steel Community (ECSC) [9,10]. These were full-scale post-flashover fires performed in a large compartment measuring 12 x 12 m in plan by 3 m height and involved a total of eight scenarios for which opening position, fire load composition and the thermal insulation of the compartment boundaries were varied. The main purpose of the tests was to characterise a range of fires for the model validation exercise performed within the scope of the NFSC programme, i.e. focusing on zone models [9-11]. A description of the experiments and the basic instrumentation

has been provided by Lennon & Moore [10]. Load cells were used to record mass loss and thermocouples were distributed throughout the compartment to monitor gas temperatures, c.f. Fig. 1. Further thermocouples were placed on and within the enclosure boundaries and supporting steelwork, including special "indicative" test sections, both with and without protection, to look at the thermal response of structural components. Zone model validation, specifically of OZone, has thus far been performed entirely in relation to the overall compartment fire temperatures derived from the tests, i.e. average of all the instantaneous thermocouple values within the compartment volume [9-11]; previous CFD model validation of the same tests has not attempted to account for thermocouple errors, though the large differences between prediction and measurement at certain lower layer positions was noted [12]. These approaches have presumed that thermocouple errors are either sufficiently small or that errors cancel out. Whilst these may be reasonable assumptions, to what extent they can be supported in the current tests has not been carefully assessed previously.

In order to more fully characterise the fires for the purposes of CFD model validation additional instrumentation was also installed, including temperature and velocity measurements in the compartment openings, together with heat flux gauges in the enclosure boundaries and in a specially-constructed box suspended near the centre of the ceiling (with a flux meter facing in each direction) [1,13], see Fig. 2. Availability of this type of information facilitates checking of key CFD predictions, such as the compartment flows and the distributions of thermal exposures. Sample results, including the corrected velocities and total heat flux measurements, are presented here.

For the model validation exercise, it is important to recognise that there are in fact two possible approaches for attempting to reconcile measured and predicted

temperatures – by correcting the former using a method such as that described here, or by doing the reverse and getting the CFD code to compute effective thermocouple temperatures [1,2]. The latter is relatively straightforward to implement [1,2], and has an advantage in terms of accounting for detailed spatial variations. This derives from the fact that the highly resolved information computed by the CFD code can be fully exploited in the thermocouple calculation, limited only by the resolution of the radiation calculation and the numerical grid. However, studies of the sensitivity of the results to variations in the assumed optical properties, which are generally poorly known, are far more cumbersome in a CFD context.

Besides their use in model validation ([1]), the availability of thermal severity maps permits a more detailed assessment of the test results than has so far been possible. Whilst gas temperatures are important for understanding the fire behaviour, their relationship with the thermal severities, which reflect the impact of the fire on structural components, is indirect. Predicted heat fluxes provide much better indicators of thermal exposures, since they accommodate the effects of remote radiation and the embedded variations in optical properties. This distinction has previously been highlighted with respect to concerns about the reproducibility of the standard fire test [14], with true thermal exposures found to be dependent on the type of furnace, and in particular the details of the geometry and the nature of the fuel (i.e. gas or oil-fired) [15], despite the fact that the same standard temperature-time relationship is rigorously adhered to. Analyses of “characteristic times” have clearly demonstrated large variations in the heating impact of nominally equivalent fires [14]. With a view to performed-based design, it is very useful to have an idea of the variation and absolute values of thermal severities that might be developed in full-scale post-flashover fires, as illustrated here.

2. Fire test programme

The ECSC NFSC2 fire tests on the BRE large compartment were conducted as part of a European collaboration to develop a new fire safety concept based on the observed behaviour of "natural" (or "real") fires. An overview of the experiments and essential measurements is provided in references 1, 9 and 10. Table 1 provides a summary of the parameters investigated.

The effective fuel load, total area of ventilation openings and overall size of compartment were fixed for all tests, c.f. Fig. 1. In each experiment, the fuel load was taken to be equivalent to 40 kg/m^2 of wood for the full floor area, with wood fuel, denoted "W" in Table 1, being 100% timber, but wood and plastic, "W+P", consisting of 80% timber/20% plastic by calorific value. A variation in ventilation was provided by moving the opening location from a full height opening at the front only, "F", to an opening over the upper half of the wall at both front and back, "F+B", whilst maintaining the same overall ventilation area of A_v=21.2m^2 (based on measured opening widths and total heights of about 3.60 and 2.95 m, respectively). Despite having equal areas these two alternatives provide for different incoming airflows and also represent different opening factors (O), due to the dependence of the latter on the square root of the opening height. These are evaluated as 0.084 and 0.060 based on the *in situ* measurements (c.f. nominal values of 0.1 and 0.07 [10]); also, the compartment floor area was a little different in test 5 due to the internal use of a light-weight walling system, resulting in a modified opening factor (O=0.066). It was intended to run two different insulation cases: "insulating" (denoted "I" in Table 1), with a nominal thermal inertia (b) value of 1600 J/m^2/s$^{1/2}$/K, and "highly insulating" (HI), with b=720

$J/m^2/s^{1/2}/K$. In practice, extra fire protection material had to be retained on the ceiling in "insulating" tests 6-8 (I+). Using the formal area-weighting method of Eurocode 1 (EC1) [16], and the ambient thermal property data provided by Lennon & Moore [10], the calculated thermal inertia values for the latter tests are about 740 $J/m^2/s^{1/2}/K$ and up to 20% lower for the highly insulating tests; under a more realistic assumption, considering only the surfaces of the upper half of the compartment, these values would be reduced to 450 $J/m^2/s^{1/2}/K$, and up to 50% lower, respectively.

2.1. Temperature

Gas temperatures were measured with thermocouples; 16 thermocouple column trees (labelled from the back left corner forwards, in rows, as G1-16) were installed in a grid pattern within the compartment, as shown in Fig. 1. In each column there were four type-K (Chromel/Alumel) bare-beaded 3mm-diameter thermocouples, capable of accurately measuring temperatures of up to about 1250°C, positioned at distances of 100, 300, 600 and 1800 mm below the ceiling, with wires attached to steel supports and withdrawn at the top via flush-fitting holes in the slab. Thermocouples were also positioned over the full height of the ventilation openings to the compartment, with similar mounting.

2.2. Heat flux

Heat fluxes were obtained using steel billets provided by the University of Ulster installed at various locations within the test compartment, c.f. Fig. 2 [1,13,17]. These devices consist of a steel cylinder, 100 mm long by 40 mm in diameter, with thermocouples installed in pre-drilled holes at distances of 2, 10, 50 and 90 mm from

the exposed face. The cylinder is surrounded by ceramic fibre insulation to promote uni-dimensional heat flow along the length. The entire assembly is encased in a tubular steel sleeve for ease of insertion into mounting holes drilled into the compartment boundaries. Total heat fluxes are computed from the measured temperatures by performing an inverse transient heat flow calculation; in the current study, it was deemed sufficient to define the temperature gradient into the depth of the billet using only the temperature values from the 2 and 10 mm thermocouple positions, though the values at the other depths could also be considered in cases with longer fire exposures. The incident flux was set equal to the conduction flux through the surface layers plus the transient heating of this region and the re-radiation estimate based on the surface temperature estimate. In order to check the calibration of the billets, reported previously by O'Connor et al [17], a Gardon gauge radiometer was also located adjacent to the billet in the back wall of the compartment in the first test.

Up to 8 steel billets were used in each test, as shown in Fig. 2. Billets 1-4 were located in the vertical exposed faces of a special insulated box mounted on the ceiling near the centre of the compartment, facing outwards in each direction at about 0.3 m below the ceiling; billet 5 was in the ceiling beside the billet box, facing downwards; and a single billet was positioned near the centre of each of the internal walls of the compartment, at a height of 1.65 m above the floor, with the exception of the "front" wall. Each billet face was set flush with the mounting surface, and blackened in an attempt to ensure a constant high emissivity throughout the tests. Thermocouples were also stationed at each billet location, projecting approximately 50 mm into the room, in order to measure local gas temperatures, which, subject to the corrections dealt with here, can be used in distinguishing the local *convective* heat fluxes.

2.3. Velocity

Velocity measurements were made in the compartment openings using McCaffrey bi-directional probes [8], with head outer diameter 16 mm, head length 32 mm and pipe internal diameter 3mm; pressure differences were logged on pressure transducers and/or micro-manometers. Different numbers of probes were used in each test, in both of the front openings, and also in the back openings where relevant; for full height openings typically eight probes were located on the vertical centreline of the doorways at distances of 50, 400, 750, 1100, 1450, 1800, 2150 and 2500 mm below the ceiling, c.f. Fig. 2.

3. Overview of fire sensitivities

Prior to any more detailed analysis it is useful to make an assessment of the main sensitivities exhibited in the test results. Lennon & Moore [10] commented upon the trends in average compartment temperatures, but mainly from the perspective of the debate on appropriate limits for the parametric temperature-time curve given in Annex B of Eurocode 1 [16], one of the concerns of the original project.

Referencing the figures in Lennon & Moore (Fig. 7 & 12-15 – though note that Test 1 values in Fig. 13 are considered somewhat unreliable, with the fire development affected by severe spalling, so this case is excluded from the comparisons), the following assessment of the sensitivities to the three parameters investigated in the tests, ventilation, insulation and fuel type, can be made:

3.1. Ventilation

Comparing tests 4 & 5 with 2 & 3, i.e. low versus high opening factors, all being highly insulating, there is a very clear delay in the growth rate, with peak temperatures attained 15-20 minutes later, for the higher opening factor cases. The peak values are also lower. These observations are supported by the comparison of a test pair with lower insulation, 7 and 8. This ventilation effect is very interesting, as it appears counter-intuitive (the ventilation-controlled fire size should be proportional to the opening factor) and is qualitatively different from the sensitivity expected from the EC1 parametric curve. The results suggest that the nature of the gas flows through openings of different geometries is more important that total ventilation areas.

3.2. Insulation

Comparing each pair of tests where compartment boundary insulation was varied reveals a very minor influence overall, with no consistent differences. However, as explained in section 2, all except the first test had very highly insulating linings in practice. Though the EC1 equation has a strong dependence on the thermal inertia value (c.f. Tables 6-7 in ref. 10), it is poorly validated for the range of these highly insulating tests, hence may not be a good guide to the expected temperature influences.

3.3. Fuel type

A very clear trend is shown here, with more rapid fire development and earlier peak temperatures developed in the tests with wood & plastic fuel. This is as expected, due to the more rapid combustion rates and higher associated soot yields of plastics, assumed to be consumed preferentially early in the test. By contrast, the EC1 equation does not have any provision to take fuel effects into account.

4. Measurement uncertainties

4.1. Temperature

It is well known that thermocouple temperatures may not be representative of the local true gas temperatures [1-7]. The reasons for this vary, though the dominant influence is normally the "radiation error" arising from the remote transfer of heat to (or from) a thermocouple bead in an environment which is locally more benign (or severe). There may also be effects due to the conduction along the length of the thermocouple wire and the transient response of the bead [3,5]. The former can result in a correction in either direction but its estimation requires a precise knowledge of the conditions along the length of the wire, which are generally insufficiently known [4]. However, the effect will usually be insignificant unless the distance between the bead and a heat sink is abnormally short [6]. Likewise, it is easy to show that the transient heating error will be small for typical fire conditions, i.e. the time-scale of the response is very short in comparison with the time-scale of the change in fire size [5,6]. Therefore, both corrections are typically neglected [3-5].

The potential significance of radiation errors has been widely recognised [1-7]. A thermocouple placed in a hot gas layer may receive radiation lower than that implied by the local gas temperature due to the influence of remote, but cool surroundings, such as a cold layer. The result is a recorded temperature slightly lower than the true gas temperature [1,3,4]. But in a lower layer, a temperature far higher than expected can often be measured [1,3-5]. This is due to the influence of radiation emanating from the distant flames and/or the hot gas layer in the environment which can be "seen" by the thermocouple, i.e. the effective "surroundings temperature" [4], or "mean radiant

temperature" [5], is much higher than the local gas temperature. In either case, the effect will tend to be more pronounced when heat transfer is dominated by radiation, as it normally is in post-flashover fires. By modelling the radiative and convective exchange between the thermocouple and the surroundings, including solid surfaces where relevant, and assuming quasi-equilibrium conditions, it is possible to predict these errors by means of energy balance theory [3-5,18]. Some authors have simply related the temperature of the surroundings to that of the compartment walls [19-21], but this approach neglects the influence of the intervening fire gases. The surroundings temperature is in reality a resultant dependent on the *distribution* of gas and surface temperatures within the region of influence, together with the optical properties of the intervening participating medium, so that there is no simple solution. However, the methodology proposed here aims to decouple the phenomena, thereby facilitating reconstruction of the underlying gas temperature field.

It should be noted that practical methods, such as the use of aspirated thermocouples, with radiation shields [4], or two-thermocouples probes, with different diameter beads [7], have been proposed to mitigate the problems of radiation errors. However, none are totally effective, and their use in large-scale tests is hindered by their complexity and expense; moreover, methods are also needed which can treat existing datasets, the majority of which were obtained with simple bare thermocouples.

4.2. Heat flux

The steel billet devices are designed to be robust heat flux meters for characterising severe thermal environments [17,13]. They measure total fluxes but since a local atmosphere temperature is recorded adjacent to each billet it is also possible, in

principle, to distinguish the convective and radiative components. The value of doing so is conditional upon assuming an accurate value for the convective heat transfer coefficient. Also, since the gas temperature measured near the billet is subject to the same uncertainties as any other, radiation errors should be corrected. However, even when the surface temperature of the billet lags well behind the gas temperature the convective fraction becomes very small after compartment temperatures have exceeded 1000°C, usually less than 10% of the total flux, and reduces still further once the billet surface temperature comes into equilibrium with the local gas-phase conditions; therefore, the distinction is generally ignored in this paper and the measured billet fluxes are assumed to represent purely radiative fluxes, though they do also encompass a small convective element.

4.3. Velocity

The measurement of velocity is very important in terms of characterising the layer heights and total compartment flows and consequently it is of most interest in the openings where these are normally well-defined. Velocity measurements are also particularly useful in helping to establish the lower layer thermocouple corrections, since it is assumed that the gas temperature will be close to ambient in locations of measured *inflow*, with any recorded differences being directly attributable to radiation error. Here, an ambient gas temperature should be referenced in the calculation of velocity from measured pressure difference, and not the local thermocouple temperature which might have departed significantly from ambient; in other locations, the best estimates of local gas temperatures need to be used, otherwise the computed velocities will also be compromised by radiation errors, though the dependence is only to a half

power of the temperature [8]. Second-order effects can also come into play, since the estimated gas temperatures themselves have a velocity dependence, via the convective heat transfer coefficient, but these relationships are generally weaker and the further corrections can reasonably be ignored.

5. Measurement corrections

5.1. Gas temperature calculations

By assuming the conduction errors for the thermocouple can be neglected, the energy balance equation may be applied:

$$\rho_{TC} c_p V \frac{\partial T}{\partial t} = \dot{q}''_{net} A \tag{1}$$

or, rearranged to represent the response of a spherical thermocouple:

$$\frac{\partial T}{\partial t} = \frac{\dot{q}''_{net} A}{\rho_{TC} c_p V} = \frac{\dot{q}''_{net} 4\pi r^2}{\rho_{TC} c_p \, {}^4\!/_3 \pi r^3} = \frac{3\dot{q}''_{net}}{\rho_{TC} c_p r} \tag{2}$$

If the net heat flux term is expressed in terms of a single effective heat transfer coefficient, h_{tot}, multiplying the temperature difference between the gases and the thermocouple bead, then Eq. (2) can be simply integrated to give a transient heating equation:

$$T = T_{gas} - \left(T_{gas} - T_a\right) e^{-\frac{3h_{tot}t}{\rho c_p r}} \tag{3}$$

The most severe challenge to the thermal response of the bead could be assumed to occur at flashover. Assuming constant values of c_p=440J/kg/K and ρ_{TC}=9000kg/m^3 for

the 3 mm Chromel/Alumel thermocouples, a characteristic convective heat transfer coefficient of 200 W/m^2/K (based on correlations below, and predicted velocities), and an initial equivalent radiative value of 150 W/m^2/K, then the thermocouple bead temperature tracks the gas temperature to within 1°C in less than 40 seconds. More exact calculations suggest that the thermal lag time is indeed generally much shorter than the most rapid measured temperature changes, hence can usually be ignored. Therefore, assuming steady-state conditions, the overall summation of the heat transfers, including net convective and radiative transfers, must equal zero, i.e.:

$$\dot{q}''_{net} = \dot{q}''_{conv} + \dot{q}''_{rad} = 0 \tag{4}$$

The individual convective and radiative exchanges are given by:

$$\dot{q}''_{conv} = h_{TC}\,(T_{gas} - T_{TC}) \tag{5}$$

$$\dot{q}''_{rad} = \varepsilon_{TC}\sigma\left(T_s^4 - T_{TC}^4\right) \tag{6}$$

where T_s is an effective surroundings temperature.

Substituting the Eqs. (5) and (6) into (4) and rearranging for the gas temperature gives:

$$T_{gas} = \frac{\varepsilon_{TC}\sigma}{h_{TC}}\left(T_{TC}^4 - T_s^4\right) + T_{TC} \tag{7}$$

The convection heat transfer coefficient, h_{TC}, can be obtained from a Nusselt number correlation, rearranged as:

$$h_{TC} = \frac{kNu}{d_{TC}} \tag{8}$$

where:

$$k = \frac{\mu c_p}{\mathrm{Pr}} \tag{9}$$

The Prandtl number is generally taken to be a constant of 0.7, following studies of non-buoyant flows [22]. The viscosity, μ, can, for instance, be calculated from Sutherland's Law [23]:

$$\mu = \frac{C_1 T^{1.5}}{T + C_2} \tag{10}$$

where the constants C_1 and C_2 are defined as 1.458×10^{-6} kg/m/s/K$^{0.5}$ and 110.4 K respectively.

The Nusselt number for a sphere can be calculated, for example, from the Williams/Kramers expression, using the Reynolds number [24]:

$$Nu = 0.37\, Re^{0.6} \tag{11}$$

where:

$$Re = \frac{\rho_{gas} U d_{TC}}{\mu} \tag{12}$$

in which the density can be evaluated from an ideal gas law correlation [25] of the form:

$$\rho_{gas} = \rho_a \left(\frac{T_a}{T_{gas}} \right) \tag{13}$$

A method is now required to approximate the effective surroundings temperature, T_s, for each thermocouple. This is achieved via a procedure which exploits the information on the current best estimates of gas temperature at the positions of each individual thermocouple to provide a numerical approximation to the radiation field seen from the position of interest. The influence of the individual contributions is weighted according to their expected radiative influence, i.e. accommodating the effects of their relative distances and the optical properties of the intervening participating

medium, characterised by the extinction coefficient, κ, assumed locally constant, together with the effective emissivity of their source regions. Note that the local thermocouple is itself included in the weighting, since this provides the best information available for characterising the local radiative field. Referencing estimated gas temperatures, T_{gas}, at thermocouples locations, TC(i=1 to n), the surrounding temperature can therefore be updated as:

$$T_s = \sqrt[4]{W_1.T_{gas,TC1}^4 + W_2.T_{gas,TC2}^4 \ldots + W_n.T_{gas,TCn}^4} \tag{14}$$

where the weighting factor, W_i is calculated using the normalised product of the transmissivity between thermocouple, *TCi*, and the thermocouple of interest and the emissivity of the volume of gas around thermocouple, *TCi*:

$$W_{i=1}^n = \frac{e^{-L_i\kappa}\left(1-e^{-\Delta L_i\kappa}\right)}{\Sigma\left(e^{-L_i\kappa}\left(1-e^{-\Delta L_i\kappa}\right)\right)} \tag{15}$$

where L_i is the total distance from the origin thermocouple, *i=1*, *to* thermocouple TC_i and ΔL_i is the path length which can be associated with the latter, measured through the gas in the same direction from the origin; for thermocouples arranged in the same direction this distance can be obtained by simply subdividing the path as L_2 for i=1, $\left(L_{n+1} - L_{n-1}\right)/2$ for $2 \le i \le n$-1, and (L_n – L_{n-1}) at i=n. Note that the transmissivity scaling is usually the dominant factor, since the weighting fundamentally decays at greater distances, whilst the emissivity weighting disappears for equally spaced thermocouples in regions of assumed homogeneous optical properties, where it is constant. The emissivity also disappears in the limiting case where a single remote thermocouple is available, since the source path length effectively becomes infinite –

which is why the emissivity of the surroundings does not normally appear in equations of the type of [7].

A characteristic value for the extinction coefficient, κ, was obtained from computations using the RadCal narrow-band model [26]. Assuming stoichiometry under ventilation-controlled burning and a soot yield of between 2% and 5% [1] this was evaluated as about unity, which is also a value approximately intermediate between the optically-thin and optically-thick limits for the characteristic length-scales of interest. The details of the actual variation in optical properties are generally unknown, and hence are considered here by means of sensitivity studies, but where measurements have, for instance, established a definite two-layer structure this can be accommodated via the weighting coefficients. This approach was used here in the compartment openings, where velocity measurements provided reliable information on layer height.

Critically, in implementing the above procedure, an iterative "boot-strapping" method is required since the current surroundings temperature estimates are used to update the local gas temperatures, which therefore all depend upon each other. The procedure is started by providing the first guess values for the gas temperatures at neighbouring thermocouple locations directly from the measured thermocouple temperatures. The resulting gas temperature estimates are then used in the next iteration, and the process is repeated until the individual estimates converge to a single self-consistent solution for the temperature field, which can be checked by entering the final values back into the governing equations. In order to overcome any numerical problems with this procedure, a conventional convergence control method was adopted, introducing a relaxation factor, r, into Eq. (7). This simply defines how much of the latest estimate to incorporate into the current approximation to the solution:

$$T_{gas} = \left[\frac{\varepsilon_{TC}.\sigma}{h}.(T_{TC}^4 - T_s^4) + T_{TC} \right].r + T_{gas-1}.[1-r] \quad (16)$$

The above method was coded in MATLAB [MATLAB® 7.4, The Mathworks, Inc., Natick, MA] in a generalised 3D fashion, and also in a simplified form, considering only interactions on individual vertical thermocouple racks, in a spreadsheet. The latter approach was found to be sufficient for the analysis of the BRE large compartment fiore test, since the horizontal couplings were generally much smaller (<5% when κ=1) due to the large 3m spacing between neighbouring thermocouple trees, and in any case horizontal temperature gradients were generally much smaller than vertical ones (see e.g. Figs. 11, 13 below). The surroundings temperatures at the billets were determined from the temperatures on the nearest thermocouple racks, together with the local billet thermocouple. In each case the temperature fields were successfully converged to within a small fraction of a degree for a reasonable number of iterations (<10) when an appropriate relaxation parameter was chosen, e.g. 0.2-0.3.

Finally, for the special case when the thermocouple bead is situated in an opening, within a region having a known inflow from the external environment, the local gas temperature can reasonably be assumed to be ambient. Hence the thermocouple correction can be found directly, and the effective temperature of the surroundings, for the radiation calculations, can be found by rearranging Eq. (7).

5.2. Radiation calculations

Having determined the corrected gas temperatures and corresponding surroundings temperatures, it is now possible to estimate the resulting associated radiance fields**:**

$$I = \frac{\varepsilon_s . \sigma . T_s^4}{4\pi} \tag{17}$$

This parameter is defined as the total radiative power per unit projected source area per unit solid angle; it differs from a heat flux which can only be defined with respect to a hypothetical solid surface, i.e. the latter enforces a directional dependence assumption whilst the former is independent of direction. However, by integrating this equation over the solid angle of a spherical surface, i.e. 4π, an equivalent radiative flux parameter, with units of W/m^2, is obtained as:

$$\dot{q}''_{rad} = \varepsilon_s . \sigma . T_s^4 \tag{18}$$

Note that the temperature used in each of these equations is the estimated surroundings temperature, T_s, and not the computed local gas temperature, since the former is a far better choice for representing the effective radiation field. Furthermore, whilst $\dot{q}''_{rad}$ is hereafter referred to simply as the "radiative flux", it must be remembered that, by referencing the surroundings temperature in the derivation, an averaging of directional effects has been enforced, so the parameter needs to be interpreted with care.

5.3. Velocity calculations

Velocities are obtained from the pressure differences measured by the McCaffrey probes using the correlation [8]:

$$\Delta p = K_t \frac{1}{2} \rho U^2 \tag{20}$$

Strictly, K_t is a function of Reynolds number, *Re*, but is relatively insensitive to variations in the range between *Re* = 1000 and 3800, where it has a theoretical value of

about 1.08. In practice, the exact value also depends on the details of the probe head geometry and can be obtained by calibration in a wind tunnel; the K_t factors obtained for the probes used in these tests varied from 1.1 to 1.3 in the high Reynolds number regime. More importantly, an accurate value of the gas density, ρ, must be referenced in each velocity computation; a thermocouple had been placed adjacent to each probe head, and these measurements are first corrected to gas temperature estimates using the method described above before determining the velocity.

6. Results

In the interests of space, detailed results are presented here only for test 8. A more comprehensive report of the results, including the other tests, will be the subject of another publication. Default emissivities of 0.9 and 0.95 were adopted for the thermocouple beads and billets, respectively.

6.1. Temperature corrections

The temperature evolution of the thermocouples at four internal vertical trees (G14, G10, G6 and G2) in test 8 is shown in Fig. 3, together with the corrected gas temperatures obtained via the methodology described above. These thermocouple trees are situated immediately to the left of the compartment centreline, located at increasing depths into the compartment, c.f. Fig. 1. The time axis runs from ignition and spans the main growth, plateau and decay phases of the fire. Progress of the high temperature region of the fire from front to back of the compartment is clear, and there is a convergence of temperatures at the respective peaks, consistent with the passage of the main “diffusion burning” interface between fuel-rich gases and fresh air (see also Figs.

13-14 below). At other times, where there is temperature stratification, there are obvious differences between the corrected and measured gas temperatures, with the thermocouples typically yielding an overestimation of the lower layer temperatures, but underestimation in the upper layer, i.e. in the expected directions.

For clarity, the thermocouple corrections, i.e. the differences between the estimated gas temperature and the measured values, ($T_{gas} - T_{TC}$), are shown directly in Fig. 4. The magnitude of the positive and negative corrections are roughly equivalent, often in the range 10-40°C but occasionally exceeding 100°C. Though these values seem small in absolute terms, they do of course correspond to a larger difference in radiative flux, due to the fourth-power dependence on temperature, i.e. about 10% for a 40ºC difference.

The sensitivity of the results to the assumed optical properties of the gases was investigated. The error bars in Fig. 4 show the values obtained for modest variation of the extinction coefficient by ±20% (i.e. κ=0.8 and 1.2, c.f. baseline value of 1.0). The influence is strong and roughly linear here, with the larger corrections indicated by the more distant ends of the error bars corresponding to the lower extinction coefficients and vice versa, i.e. corrections are suppressed in optically-thick regions, as expected. However, this sensitivity is found only to be important in the region of intermediate extinction coefficients, tailing off rapidly as the limits of optically-thin and optically-thick are approached in each direction, e.g. there is little further change (<13%) below κ=0.1 and above κ=5. The baseline corrections, for κ=1, are approximately halfway between these two limits, i.e. the modelled values are effectively doubled in the optically-thin limit but reduced back to the original thermocouple values in the optically-thick limit, where no radiative exchange is possible.

The resultant optical property sensitivities derived from the model predictions were cross-plotted with an equivalent variation in the underlying gas transmissivity, Eq. 15, and found to match very well by adopting a characteristic length-scale of 0.65m. This is a useful general result confirming that the key factor determining the behaviour of the full coupled system is the effective gas transmissivity. This parameter can of course be varied by changing the thermocouple distribution and density.

The influence of other model parameters was also investigated in sensitivity studies. Variation of the thermocouple emissivity, either side of the assumed value of 0.9, had a similar effect to the optical property variation mentioned above. Changing the convective properties by altering the thermocouple bead diameter or the local velocity by a factor of two in either direction, thereby altering the Reynolds number (Eq. 12) and hence convective heat transfer coefficient, produced error bars similar to those for the optical property variations, but about 70% bigger.

6.2. Opening velocity and temperature corrections

In order to correct both the temperatures and the velocities in the opening the local flow direction must be taken into account. Where a probe is located in a strong incoming airflow it can reasonably be assumed that the local gas temperature does not differ appreciably from ambient, hence the thermocouple error can be obtained directly by difference; a correction procedure is still required for hot layer adjustments and the method adopted was the same as that described earlier, but with the emissivity explicitly set to zero, and transmissivity to unity, in regions of known ambient gases.

The corrected gas temperatures are shown in Fig. 5 at the position of each velocity probe (see section 2.3 above) and the difference between calculated and recorded

temperatures ($T_{gas} - T_{TC}$) is shown in Fig. 6. The graph displays curves for the locations generally in the hot layer, whilst individual data points are plotted for the lower positions, due to the scatter which results from occasional local oscillations in flow direction. The error bars indicate the same bounds on the influence of optical properties.

The results demonstrate that the thermocouple errors can be very large indeed in the inflow, but also that they can be rather greater in the hot layer here than they are within the depth of the compartment (Fig. 6, c.f. Fig. 4). Both findings are as expected in view of the stronger underlying temperature stratification in the opening. In the hot layer, the sensitivity of the results to optical property variations is of a similar magnitude as it was internally, whilst the uncertainties in the measured ambient inflow regions are generally negligible, due to the fact that the gas temperature is assumed unambiguous here.

Fig. 7 shows the corrected velocity histories, with the same error bar assumptions. Also included are the probe 8 values using uncorrected temperatures, showing the large impact of the temperature correction on velocity in the lower layer. Differences in the hot layer were much smaller, averaging <2%, but locally up to 5%. The optical property uncertainties are clearly much smaller than for temperature, <1% in the hot layer, due to the indirect dependence of velocity on temperature, via on the square root of the density (c.f. Eq. 20). In the optical thickness limits, the same maximum percentage difference did not exceed 6% in either direction.

6.3. Heat flux comparisons

Three billets were used in test 8, in the ceiling (billet 5) and in the left-hand and right-hand sidewalls (billets 7 and 8, respectively), c.f. Fig. 2. Comparisons of the measured total fluxes and values computed from gas temperatures, both from the

thermocouple local to the billet and from the nearby thermocouple trees, are presented in Figs. 8-10. For the thermocouple trees, both the measured and corrected temperatures were used for comparison, and for the latter the same optical property variations are again indicated by the error bars. The convective fluxes are also plotted for reference, based on a modelled convective heat transfer coefficient of 6 $W/m^2/K$ [1].

For the ceiling billet, Fig. 8. there is a reasonable agreement between the different flux calculation methods, with some underprediction from the billet thermocouple but overprediction from the thermocouple tree values later in the fire. This correspondence is mainly due to the fact that the nearby thermocouple trees include measurement points just 100 mm below the ceiling surface, which are therefore well able to characterise the local heating conditions.

The results for the sidewall locations, Figs. 9-10, show quite different heating trends, reflecting asymmetry in the fire development. Here, there are much larger discrepancies between the measurements and computed values, with the values derived from the nearby thermocouples being consistent overpredictions. This was the case whether or not the corrected gas temperatures were used, with most values also well outside the error bars for optical property variation, but it is not unexpected due to that fact that the minimum distance to the nearby tree thermocouples was 1.75m. The effect of using corrected temperatures is very low at this intermediate height, and similar differences were found by using a corrected temperature for the billet thermocouple (not shown). However, apart from billet 7 during the decay phase, the overall agreement is within the experimentally determined accuracy of this measurement device [17,13]. Comparisons of the fluxes measured by the Gardon gauge and back wall steel billet in test 1 of the current series were consistent with these, showing an average discrepancy

within 20% [13]. The estimated convective fluxes are seen to be low throughout, and insignificant in the comparisons.

6.4. Temperature and radiative flux maps

Spatial variation in the thermal fields is illustrated by means of contour plots on planes within the compartment, as described in the following sub-sections. Three plane cross-sections are examined: 1. into the depth of the compartment, on the doorway centreline (section AA, c.f. Figs. 1-2), 2. across the width of the compartment, at mid-depth (line 2, c.f. Figs. 1-2), and 3. just below the compartment ceiling. In each case, plots are produced at 10 minute intervals between 10 and 40 minutes, in order to capture the evolution of main post-flashover stage of the fire, c.f. Figs. 3-10. Maps of gas temperature and equivalent radiative flux fields are shown; the latter parameter was obtained as described in section 5.2 above. The plots were created using SigmaPlot [SigmaPlot® 10.0, Systat Software Inc., San Jose, CA]. Since the sampled points were not distributed regularly 3D data smoothing was first performed, using the Loess smoother (tricube weighting and polynomial regression); a first-degree polynomial was adopted with a sampling proportion of 0.4 (i.e. the fraction of the data points used to compute each smoothed value) and a "nearest neighbours" bandwidth method. Though this method does not guarantee to fit the surface through each individual data point it provides charts which are relatively easy to read yet with acceptable residual values, i.e. a small difference between fitted points and original data; the latter averaged 3% for temperatures and 10% for effective fluxes, being greatest in regions of strong gradient, i.e. the side elevations of Figs. 11-12, but very low for the front elevation of Figs. 13-14. Note that the values outside the region of sampled data points are indicative only; in

particular, the region between the lowest thermocouple and the floor was treated by equating the assuming the same value at both positions, even though there were no measurements at the floor; this region is highly uncertain anyway as the flow was significantly impeded by the crib structures during much of the test.

6.4.1. Plane through opening

A plot of the estimated gas temperatures reveals clear evidence of stratification, particularly near the opening (on the right of the plot). The highest temperatures are initially located towards the front where the main burning zone is located due to the proximity of the ventilation (Fig. 11a). The influence of a strong inflow of ambient air is seen in the lower section of the doorway. As fuel begins to burn out there is an obvious progression of the highest temperature region (>1100°C) towards the rear of the compartment and stratification is generally reduced.

The equivalent radiative flux plot (Fig. 12a) shows stronger gradients and peak regions offset more towards the middle of the compartment, where there are longer radiation path lengths. The highest fluxes, exceeding 200kW/m^2, are found towards the front of the compartment early in the test. Regions of peak radiative flux progress towards the rear of the compartment (Figs. 12 b-d), and are much more clearly defined that the peak temperature regions, partly due to the fourth-power temperature dependence of the radiation.

6.*4.2. Plane across width, mid-depth*

The gas temperature profiles displayed in Fig. 13 also show some vertical stratification, particularly at 10 minutes. There is considerable asymmetry in the

distribution, with burning on this plane initially focussed on the right of the test compartment, before moving more to the left by 30 minutes, consistent with the flux results described above, c.f. Figs. 9 -10.

The equivalent evolution of radiative fluxes with time is shown in Fig. 14. Again, stronger gradients are shown, with the peak thermal exposures some distance below the ceiling. For these cases, the predicted values can also be compared directly with the billet data for the left and right sidewalls, indicated on the plots at the locations of the black squares. The results show a fair agreement, considering the known uncertainties, with the asymmetry of the results for 20 and 30 minutes captured reasonably well.

6.4.3. Plane below ceiling

Plots of the estimated gas temperatures just below the ceiling are shown in Fig. 15. Due to the presence of a hot smoke layer, the temperatures in this region are consistently high – all in excess of 600^{o}C. However the results still reveal the dynamic nature of the fire. Highest temperatures are initially seen at the opening, exceeding 1300°C, but then progress towards the rear of the compartment as the fuel burns out. The asymmetry noted in Figs. 9 &10, and 13, is again apparent, with higher temperatures towards the right sidewall still apparent at 40 minutes.

Fig. 16 shows strong gradients of radiative flux over the entire ceiling at all stages of the fire. The peak exposure region can be seen to progress back from the compartment openings on the right; at 10 minutes the values are relatively modest despite the high gas temperatures; by 20 minutes there are two peaks, one in the upper right corner of the opening but another further back into the compartment, the latter being far more pronounced than on the temperature map (Fig. 15). High fluxes persist at

40 minutes, concentrated towards the rear of the compartment. Throughout, the discrepancy between the peak and minimum fluxes exceeds a factor of three, showing that even during the post-flashover stage significant variations of thermal exposures may be present.

6.4.4. Comparison with averaged test results

For comparative purposes, the average compartment temperatures obtained on the basis of the corrected gas temperatures and the original thermocouple readings were computed and cross-plotted, see Fig. 17. There was very little difference in overall terms, with discrepancies during the burning plateau averaging 7°C. The reason for such a small effect is predominantly due to the intrinsic error cancellation in the thermocouple estimates – energy lost from one part of the domain is captured in another and differences are only large locally. This has clear implications for the use of averaged measured temperatures in validation of simple fire models.

7. Discussion and conclusions

The model results indicate the possible significance of radiation errors in large post-flashover fires of this type. These can be particularly large in the lower layer, especially in ambient inflow regions, but they cannot be neglected anywhere that gradients exist in the underlying gas temperature field. Corrections must also be considered for gas velocities, particularly in inflow regions where they can be in error by over 50% due to radiation effects.

The highest temperature corrections are found towards the optically-thin limit, with a reduction towards zero in the optically-thick limit. In practice, the sensitivity to the assumed optical properties is very small beyond certain extinction coefficient bounds, which are related to the spacing of the sampling locations, i.e. the number of thermocouples. A general result is that if the optical properties of combustion gases can be estimated in advance then the likely significance of temperature corrections can be related to a characteristic length-scale; the latter is directly related to the typical spacing of the measurement points and can be linearly reduced by employing more thermocouples. This type of assessment might also indicate that engulfed region corrections will be negligible when opacity is large, i.e. in smoky combustion gases, so can be neglected. For fires of uncertain optical properties, as in the current case, departures from the assumptions of the correction methodology can be explicitly addressed, as illustrated here.

Overall, the results presented are consistent with the earlier analysis which indicated that very severe thermal environments were possible in this type of well-insulated and well-ventilated compartment [10,13]. Gas temperature peak at over 1300°C, associated heat fluxes reach nearly 300 kW/m^2 and corrected opening velocities exceed 13m/s. The observed rapid rate of temperature rise is consistent with the inclusion of plastic in the fuel.

Besides the ultimate establishment of a self-consistent and reliable dataset of physical parameter values for use in model validation, with a reconstruction of the gas temperature field, one of the key motivations of this work was to look at the thermal exposure distributions within post-flashover fires. Conventionally, these are assumed to be uniform, or at best partitioned into two layers, but this simplification is not well

supported by these results. Strong variations were observed in the gas temperature distributions, with some of these being further enhanced in the related radiative flux distributions which frequently showed instantaneous differences of over a factor of three in a single plane.

Heating potential of fires is often assessed purely in terms of gas temperatures, or if test data are used, thermocouple temperatures. The inadequacy, locally, of the latter approach for gases which are not optically thick has been clearly shown here. A more useful parameter for characterising thermal exposures is the effective radiative flux, i.e. the total radiant energy per unit area, which would theoretically be incident upon a structural member if located there, i.e. neglecting directional effects and under the assumption that the component is small, not significantly interfering with the flowfield. It is shown that the distribution of radiative fluxes may be markedly different from that of gas temperature, due to the influence of radiative transfers and temperature dependencies. The locations where gas temperatures peak at a macroscopic level, typically near openings or at diffusion burning interfaces, can be distinctly offset from the regions of peak radiative fluxes, which tend to occur deeper into the fire. This is because the remote environment may have a strong influence on the thermal exposures, these being enhanced where there are long path lengths through high temperature combustion products, but suppressed where ambient environments exert a moderating influence. In this respect, the radiative flux parameter mirrors the behaviour of thermocouples in radiatively-dominated environments; though the latter do not provide a direct measure of thermal severities, i.e. the likely impact of the fire on structural components, they do provide a idea of the distribution of heating and can be used to estimate effective radiative fluxes.

Finally, whilst local gas temperatures might not be well represented by thermocouple measurements, values which are averaged over the whole fire region seem to provide a very good approximation to the average gas temperatures. Hence, the previous work on zone model validation which was conducted with respect to the NFSC2 tests [9-10], using only averaged thermocouple temperatures to characterise the heating, is well supported by this more detailed analysis.

Acknowledgments

The financial support of the Research Fund for Coal and Steel (RFCS), formerly ECSC, is gratefully acknowledged, together with the contributions of all the project partners, in particular Suresh Kumar, Tom Lennon & Norman Marshall at BRE and Simo Hostikka at VTT. The authors also wish to thank staff (formerly) of the University of Ulster who assisted with the heat flux measurements, in particular David O'Connor, Brian Morris and Lee Masson. Cecilia Abecassis-Empis programmed the MATLAB implementation of the method.

References

[1] Kumar S, Welch S, Miles S D, Cajot L-G, Haller M, Ojanguren M, Barco J, Hostikka S, Max U & Röhrle A. Natural Fire Safety Concept - The development and validation of a CFD-based engineering methodology for evaluating thermal action on steel and composite structures. 2005. Office for Official Publications of the European Communities, Luxembourg. Technical steel research. Steel structures. ECSC Research 7210-PR-184, 1999-2002, EUR 21444 EN, 150 pp., ISBN 92-894-9594-4.

[2] Wen JX, Huang LY & Roberts J. The effect of microscopic and global radiative heat exchange on the predictions of compartment fires. Fire Safety J 2001;36:205-223.

[3] Luo M. Effects of radiation on temperature measurement in a fire environment. J Fire Science 1998;15:443-461.

[4] Blevins LG & Pitts WM. Modelling of bare and aspirated thermocouples in compartment fires gradients). Fire Safety J 1999;33:239-259.

[5] Francis J & Yau TM. On radiant network models of thermocouple error in pre and post flashover compartment fires, Fire Tech 2004;40:277-294.

[6] Bradley D & Matthews KJ. Measurement of high gas temperatures with fine wire thermocouples, J Mechanical Engineering Science 1968;10(4):299-305.

[7] Broheza S, Delvosalle C & Marlair G. A two-thermocouples probe for radiation corrections of measured temperatures in compartment fires, Fire Safety Journal 2004;39:399-411.

[8] McCaffrey BJ & Heskestad G. A robust bidirectional low-velocity probe for flame and fire application, Combust Flame 1976;26(1):125-127.

[9] Schleich J-B, Cajot L-G, Pierre M, Moore D, Lennon T, Kruppa J, Joyeux D, Hüller V, Hosser D, Dobbernack R, Kirchner U, Eger U, Twilt L, Van Oerle J, Kokkala M, & Hostikka S. Natural fire safety concept – full scale tests, implementation in the Eurocodes and development of an userfriendly design tool. 2003. Office for Official Publications of the European Communities, Luxembourg. ECSC Research 7210-060, 1997-2000, EUR 20580 EN.

[10] Lennon T & Moore D. The Natural Fire Safety Concept - full-scale tests at Cardington. Fire Safety J 2003;38:623-643.

[11] Cajot L-G & Schleich J-B. Natural fire safety for buildings. Proc. 9th Interflam conference, Interscience Communications Ltd, London, 359-368. 2001.

[12] Pope ND & Bailey CG. Quantitative comparison of FDS and parametric fire curves with post-flashover compartment fire test data, Fire Safety J 2006;41:99-110.

[13] Masson L. The use of an instrumented steel billet to measure incident heat flux. 2003. MSc thesis, University of Ulster.

[14] Paulsen OR & Hadvig S. Heat transfer in fire test furnaces. Fire and Flammability 1977;8:423-442.

[15] Welch S & Rubini P. Three-dimensional simulation of a fire resistance furnace. Fire Safety Science - Proc. 5th Int. Symp., IAFSS, 1009-1020. 1999.

[16] Eurocode 1: Actions on structures, Part 1.2: General actions - actions of structures exposed to fire, EN 1991-1-2:2002, British Standards Institution.

[17] O'Connor DJ, Morris B & Silcock GWH. Flux measurement in real and standard fires, in Fire, Static, and Dynamic Tests of Building Structures: Proceedings of the

second Cardington conference: Part1: BRE Fire Programme, Eds. Armer, G. S. T. & O'Dell, T., 1997, Spon Press (UK), 286 pp., ISBN 0419216804

[18] Incropera FP & DeWitt DP. Fundamentals of heat and mass transfer. 2002. John Wiley & Sons, Inc., New York.

[19] Holman JP. Heat transfer. 1997. McGraw-Hill Book Co., London.

[20] Carvalho JA & Santos WFN. Radiation errors in temperature measurements with thermocouples in a cylindrical combustor. Int. Comm. Heat Mass Transfer 1990;17:663-673.

[21] Jones JC. On the use of metal sheathed thermocouples in a hot gas layer originating from a room fire. J Fire Science 1995;13:257-260.

[22] Jones WP & Whitelaw JH. Calculation methods for reacting turbulent flow: A review. Combust Flame 1982;48:1-26.

[23] Anderson D, Tannehill J & Pletcher R. Computational fluid mechanics and heat transfer. 1994. McGraw-Hill, New York.

[24] McAdams WH. Heat transmission. 1954. McGraw-Hill, New York.

[25] Drysdale DD. An introduction to fire dynamics. 2000. John Wiley & Sons Ltd, Chichester.

[26] Grosshandler W. RadCal: A narrow band model for radiation calculations in a combustion environment. NIST Technical Note (TN 1402), National Institute of Standards and Technology, Gaithersburg, Maryland 20899, 1993.

Table 1

Details of ECSC NFSC2 fire tests in BRE large compartment

Test number	1	2	3	4	5	6	7	8
Fire load type	W	W	W+P	W	W+P	W	W+P	W+P
Boundaries	I	HI	HI	HI	HI	I+	I+	I+
Opening	F	F	F	F+B	F+B	F+B	F+B	F

Key: W = 100% wood

W+P = 80% wood, 20% plastic

I = compartment lining – "insulating" ($b \approx 1600$ J/m^2/s$^{1/2}$/K)

HI = compartment lining – "highly insulating" ($b < 700$ J/m^2/s$^{1/2}$/K)

I+ = compartment walls – "insulating", ceiling – "highly insulating", ($b < 750$ J/m^2/s$^{1/2}$/K – see text)

F = opening at the front only (O=0.084)

F+B = openings at both front and back (O=0.060; in test 5, O=0.066)

where:

b is the thermal absorptivity ($=\sqrt{k\rho c}$)

O is the "opening factor" ($=\frac{A_v\sqrt{h_{eq}}}{A_t}$)

where:

A_v is the total area of vertical openings on all walls

h_{eq} is the weighted average of window heights on all walls, and total area of compartment (i.e. walls, ceiling and floor, including openings).

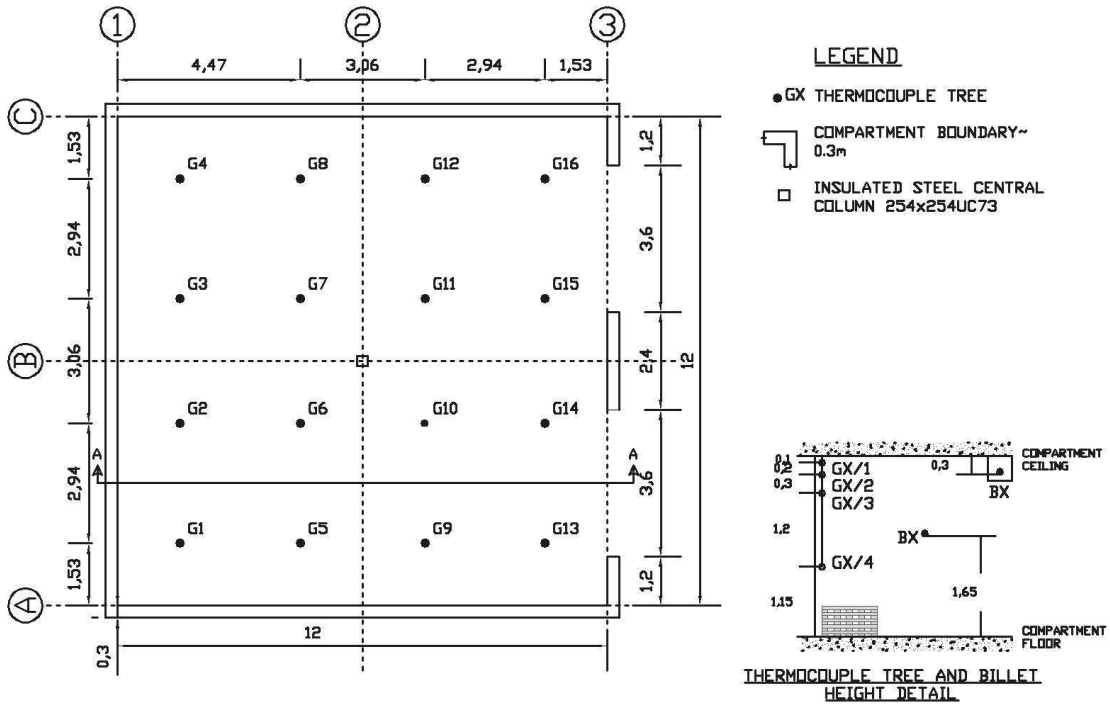

Fig. 1. Plan and elevation of fire compartment showing dimensions and thermocouple tree locations; ventilation openings on the right (test 8).

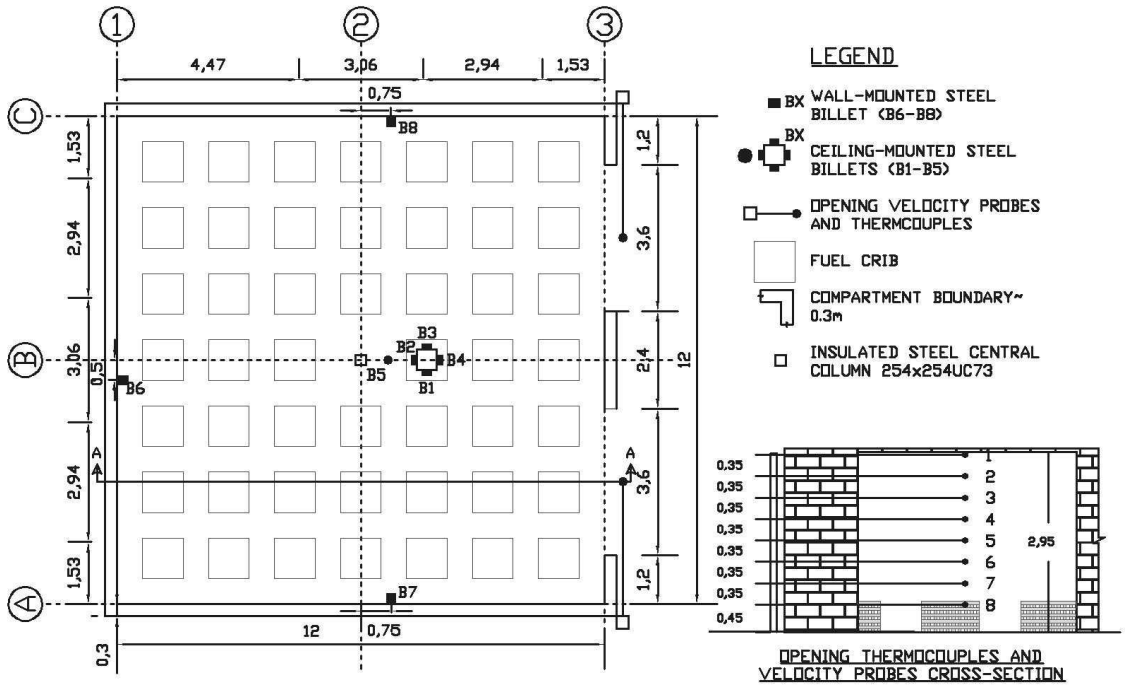

Fig. 2. Plan and elevation of the fire compartment showing locations of cribs, steel billet total heat flux measurement devices and velocity probes (test 8).

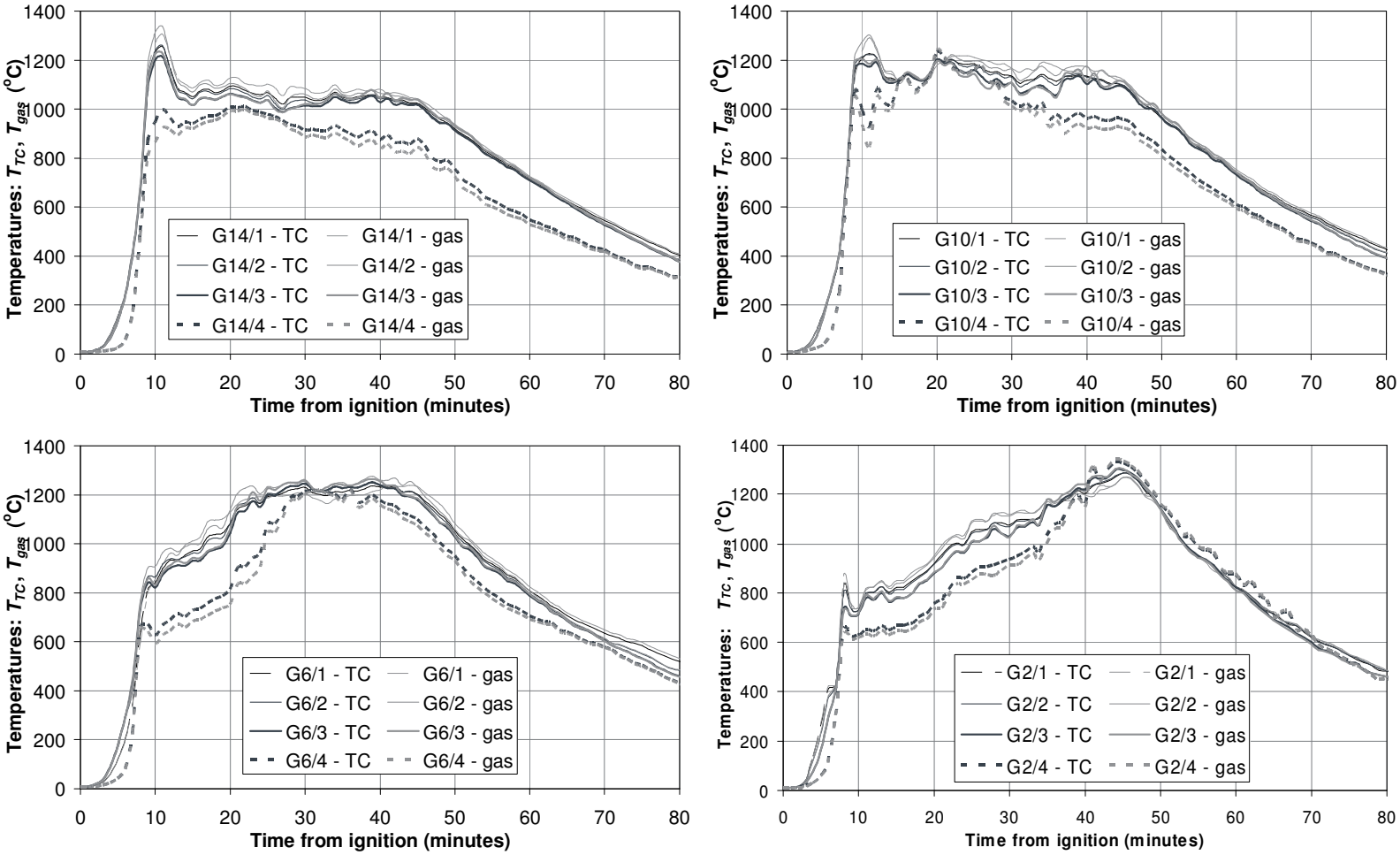

Fig. 3. Comparison of corrected and measured gas temperatures for thermocouple trees G14, 10, 6 & 2 (test 8); see Fig. 1 for exact locations.

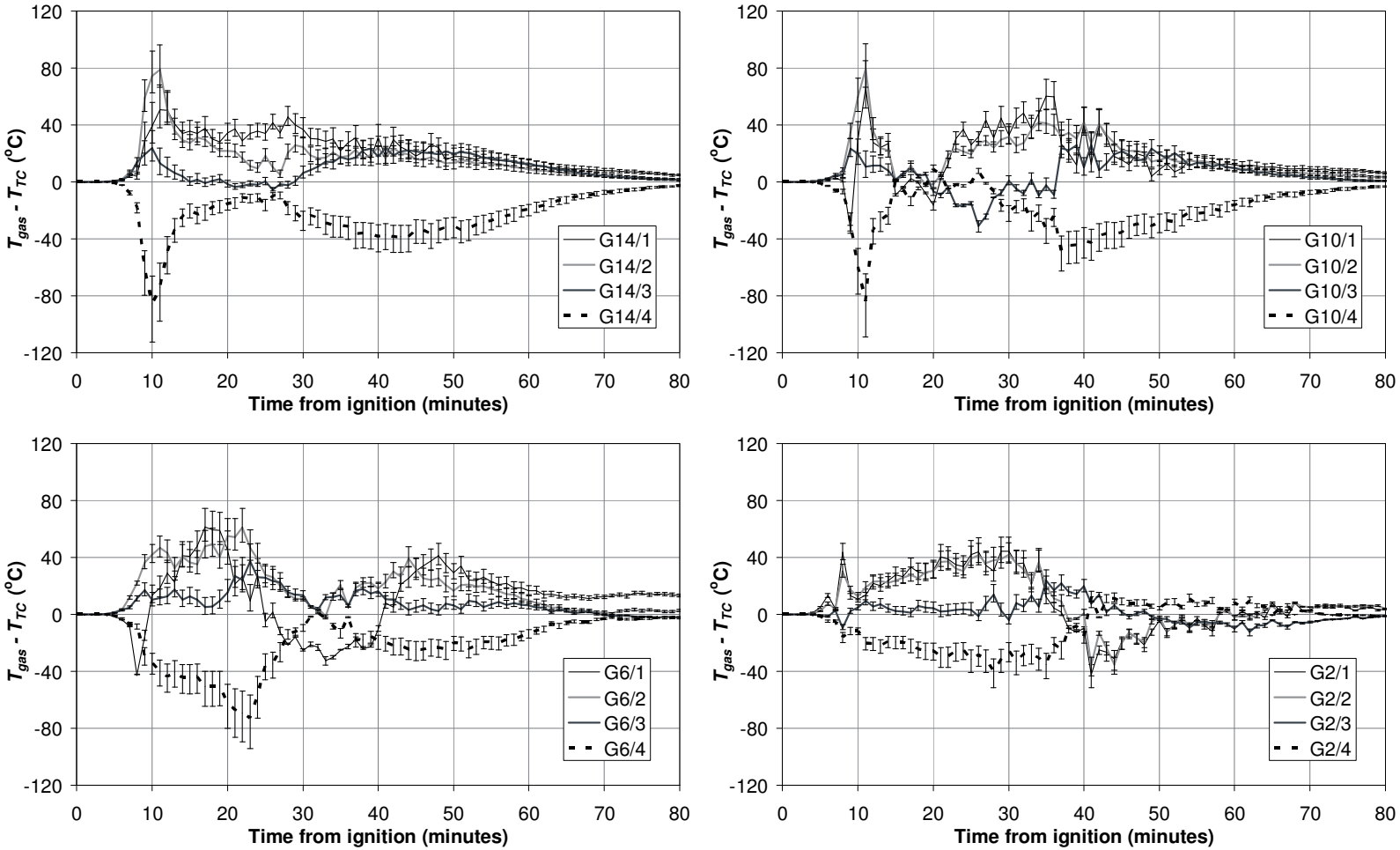

Fig. 4. Temperatures corrections (T_{gas}-T_{TC}) for thermocouple trees G14, 10, 6 & 2 (test 8); error bars indicate extinction coefficient bounds (κ=0.8 and 1.2); see Fig. 1 for exact locations.

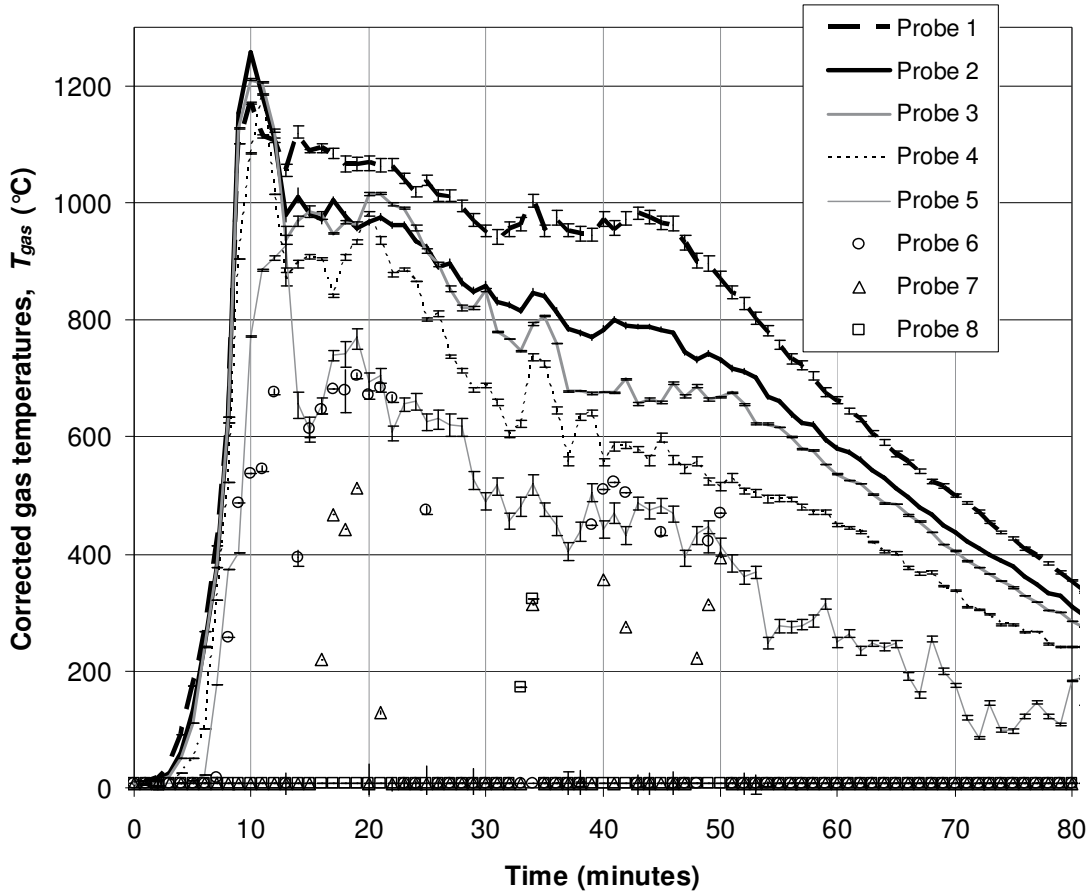

Fig. 5. Corrected gas temperatures, T_{gas}, at the velocity probe locations in the right-hand opening (test 8); error bars indicate extinction coefficient bounds (κ=0.8 and 1.2); see Fig. 2 for exact locations.

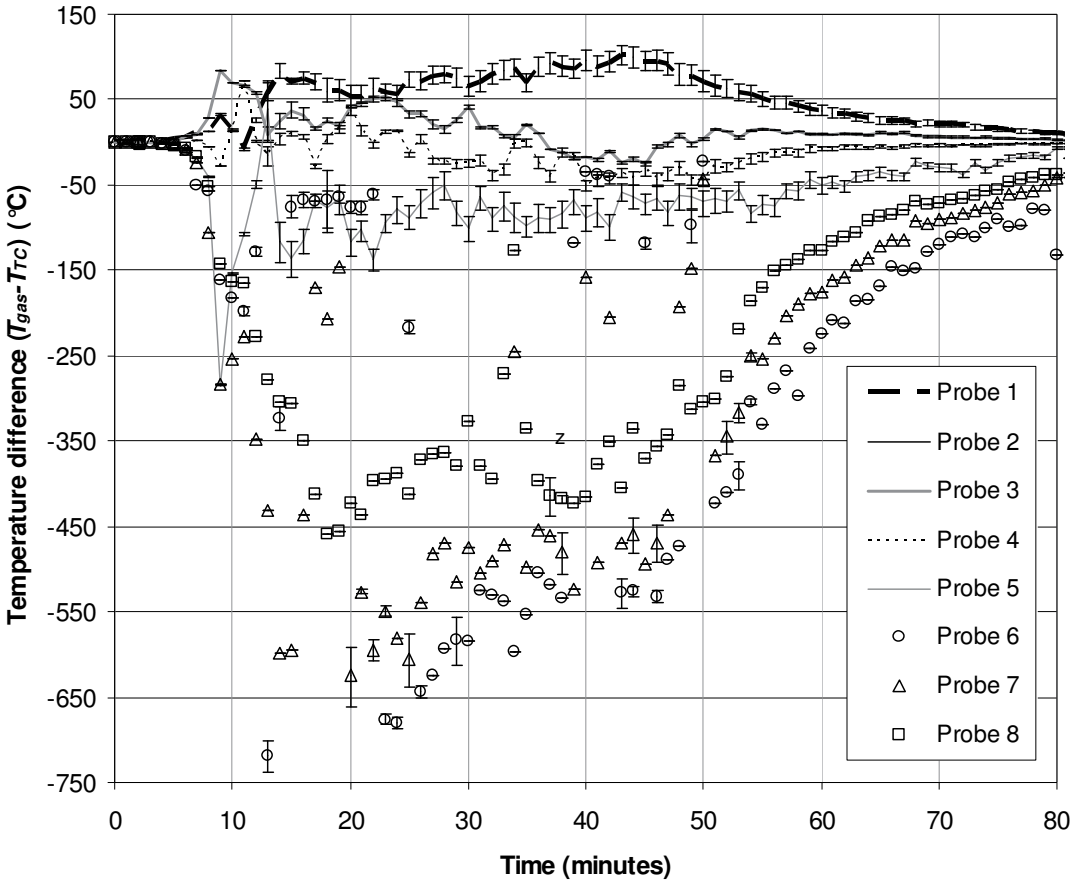

Fig. 6. Temperature differences, ($T_{gas} - T_{TC}$), at the velocity probe locations in the right-hand opening (test 8); error bars indicate extinction coefficient bounds (κ=0.8 and 1.2); see Fig. 2 for exact locations.

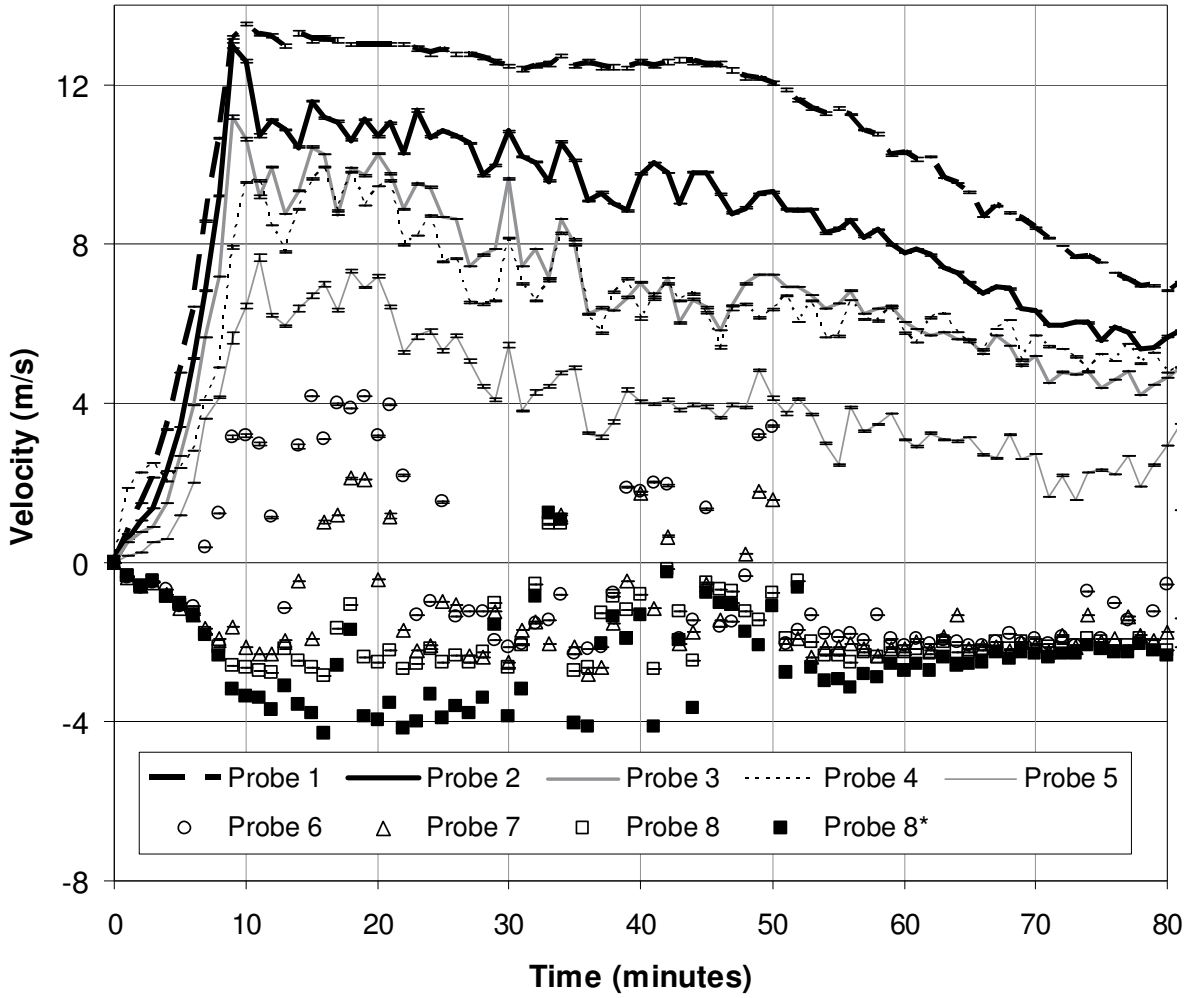

Fig. 7. Corrected gas velocities at the velocity probe locations in the right-hand opening (test 8), with comparative uncorrected values for Probe 8*; error bars indicate extinction coefficient bounds (κ=0.8 and 1.2); see Fig. 2 for exact locations.

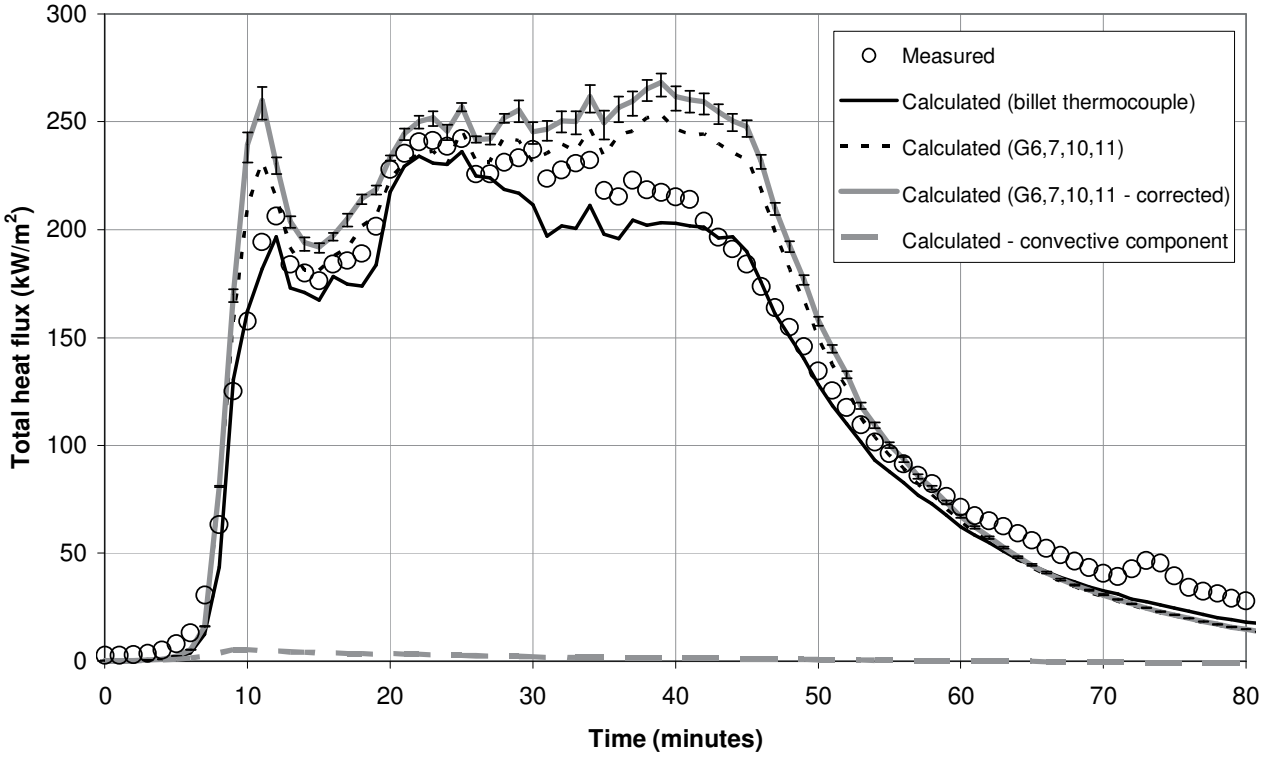

Fig. 8. Comparison of total heat flux measurements and values calculated from local billet thermocouple, and local thermocouple trees (G6,7,10,11), with & without correction (billet 5 – ceiling, test 8).

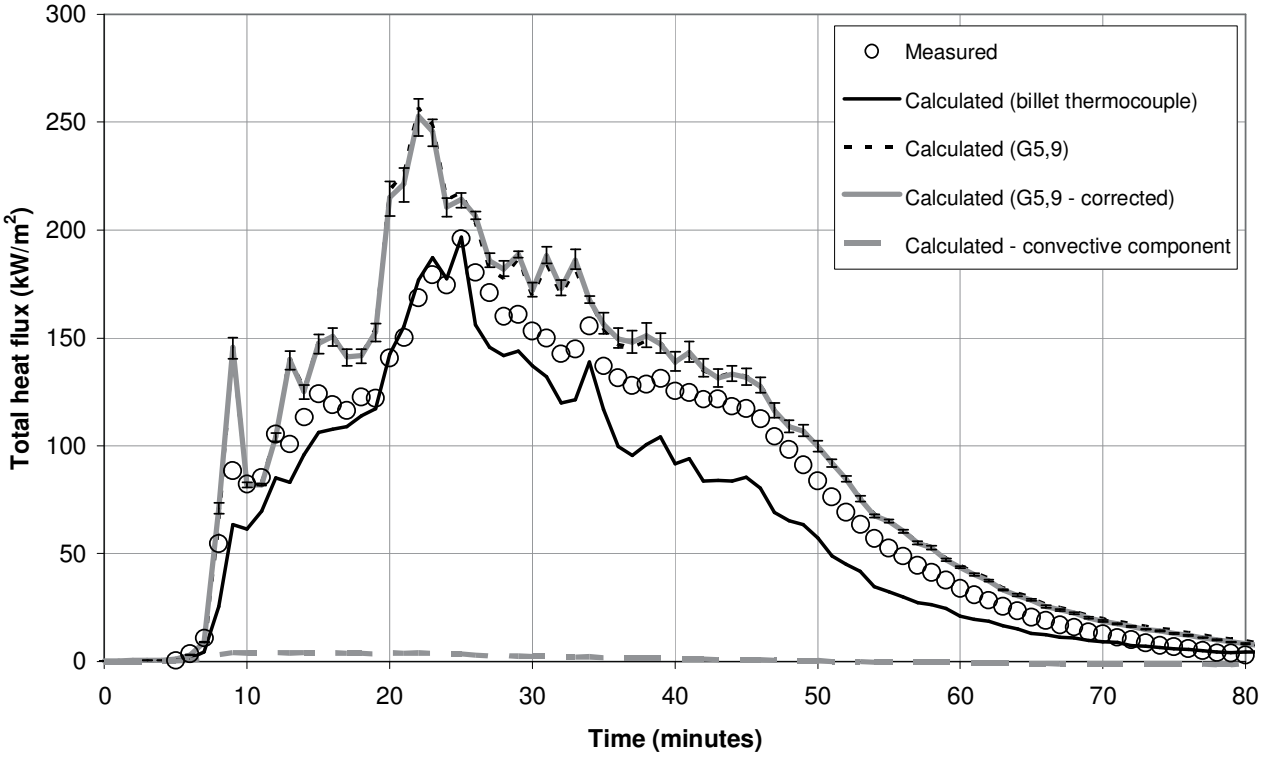

Fig. 9. Comparison of total heat flux measurements and values calculated from local billet thermocouple, and local thermocouple trees (G5,9), with & without correction (billet 7 – left sidewall, test 8).

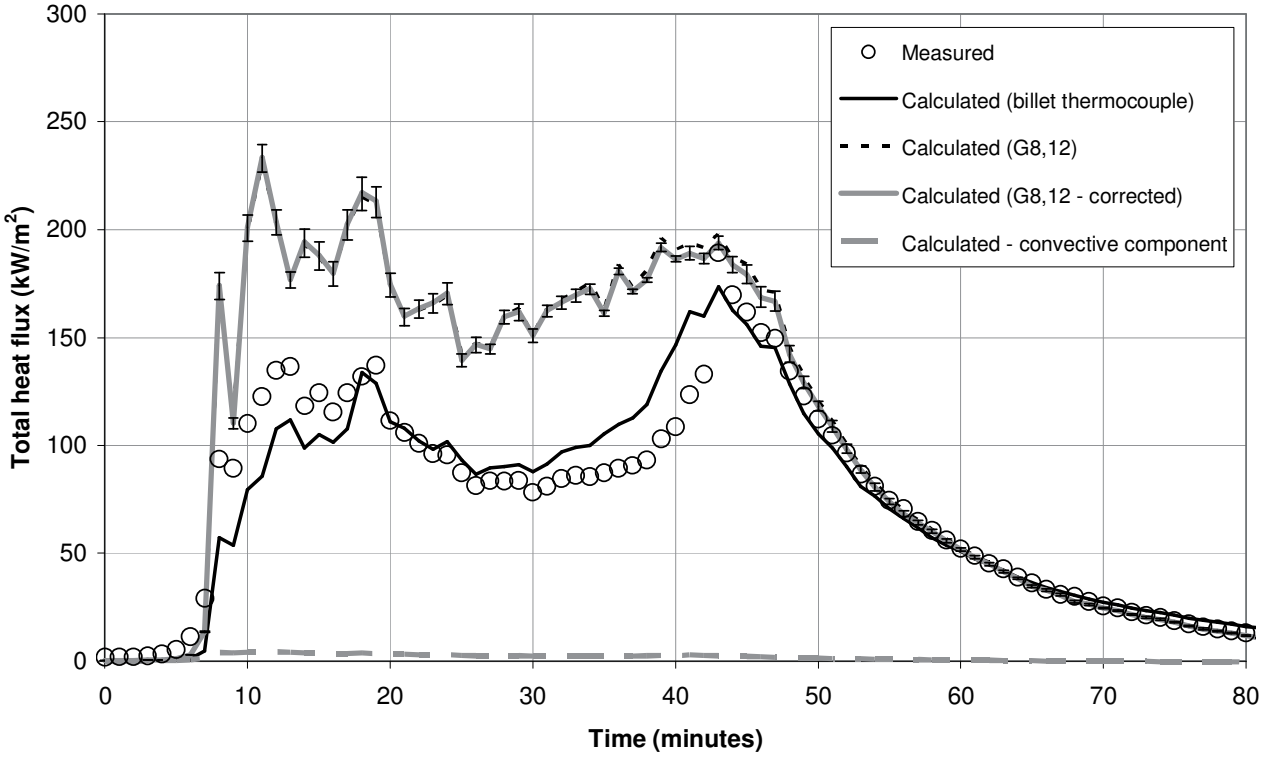

Fig. 10. Comparison of total heat flux measurements and values calculated from local billet thermocouple, and local thermocouple trees (G8,12), with & without correction (billet 8 – right sidewall, test 8).

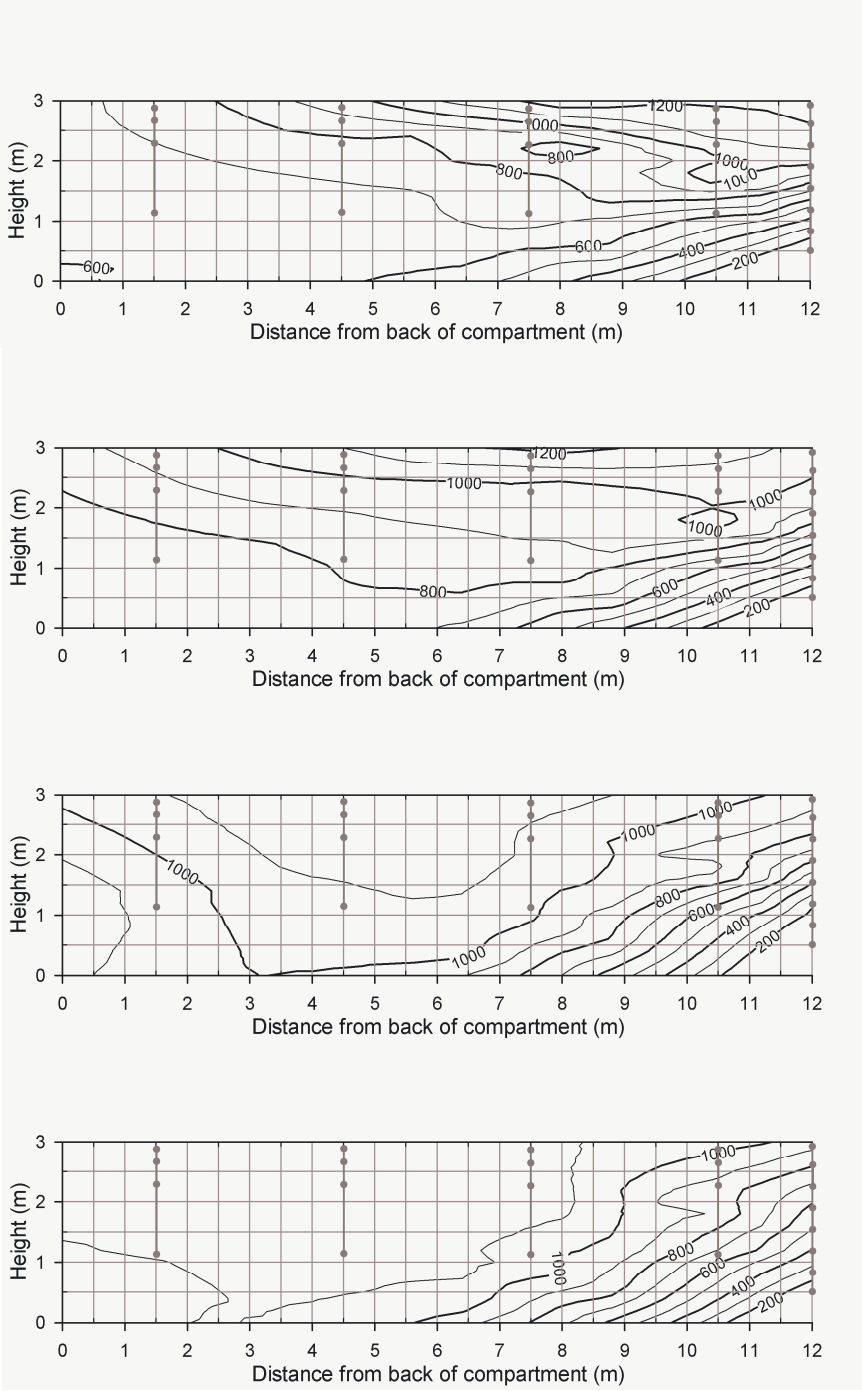

Fig. 11. Gas temperature map over cross-section through compartment (section AA, Figs. 1-2) from back wall – left, to doorway – right (test 8); contour labels in °C.

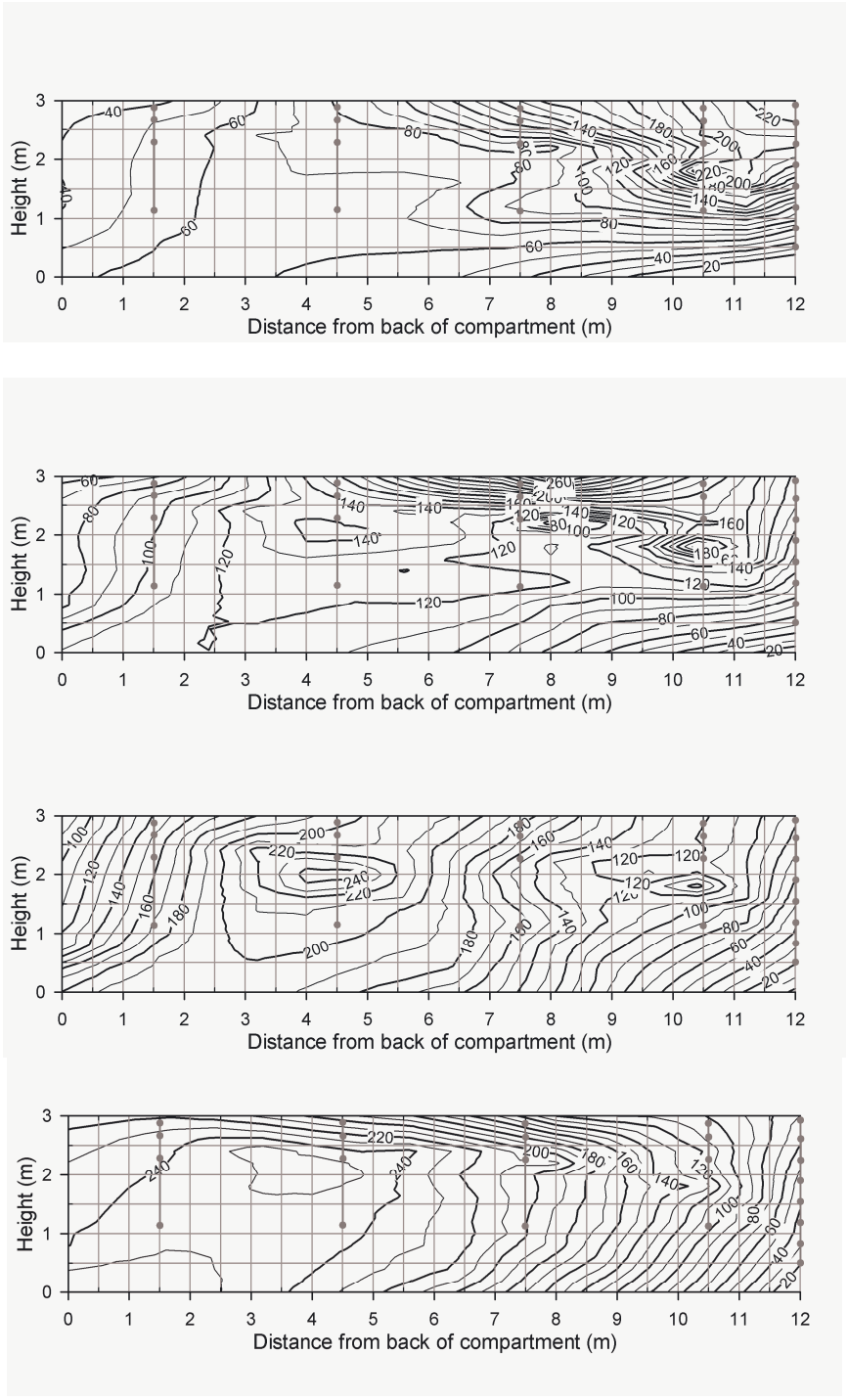

Fig. 12. Heat flux map over cross-section through compartment (section AA, Figs. 1-2) from back wall – left, to doorway – right (test 8); contour labels in kW/m^2.

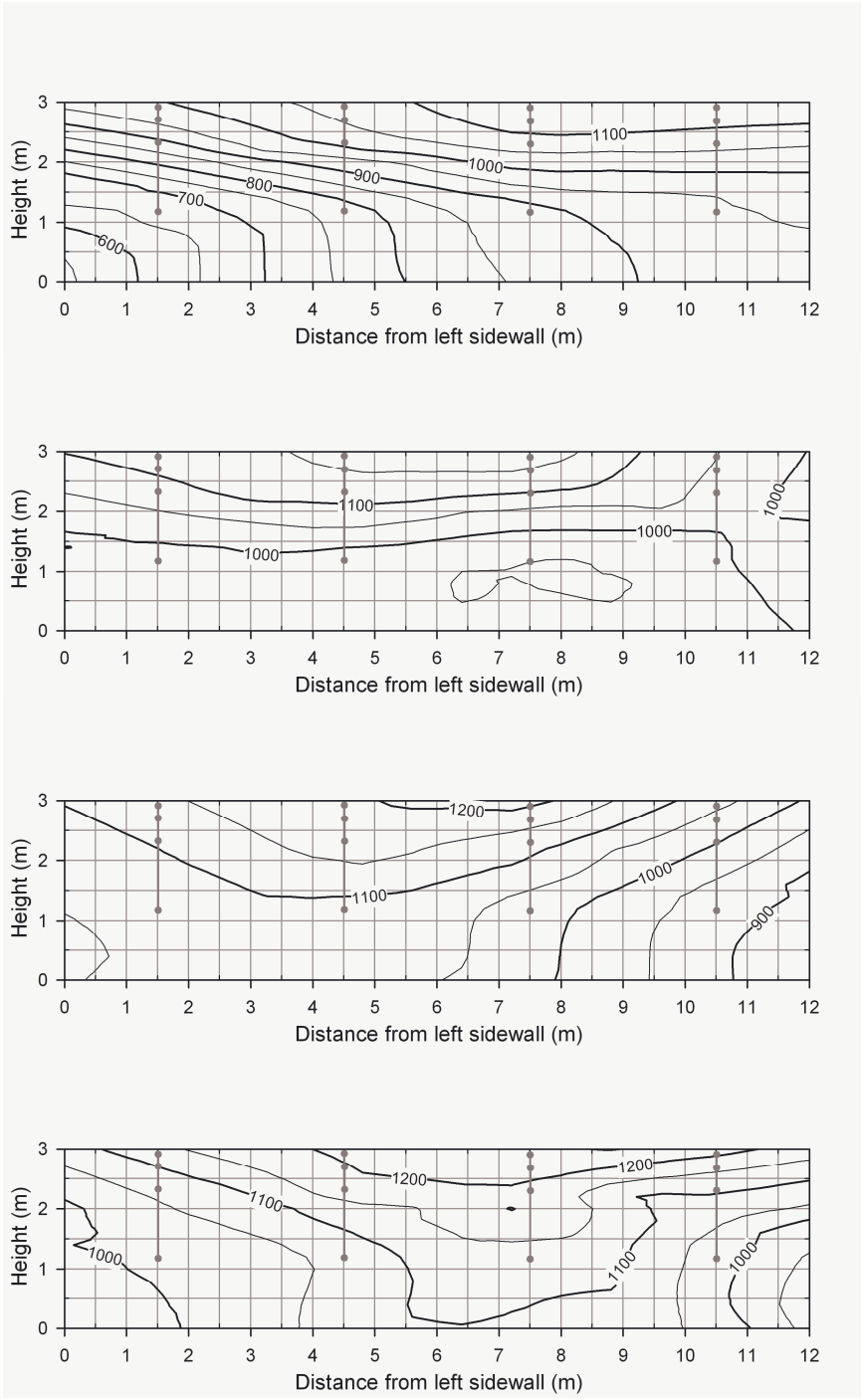

Fig. 13. Gas temperature map over cross-section through centre of compartment (line 2, Figs. 1-2), viewed from front, (test 8); contour labels in °C.

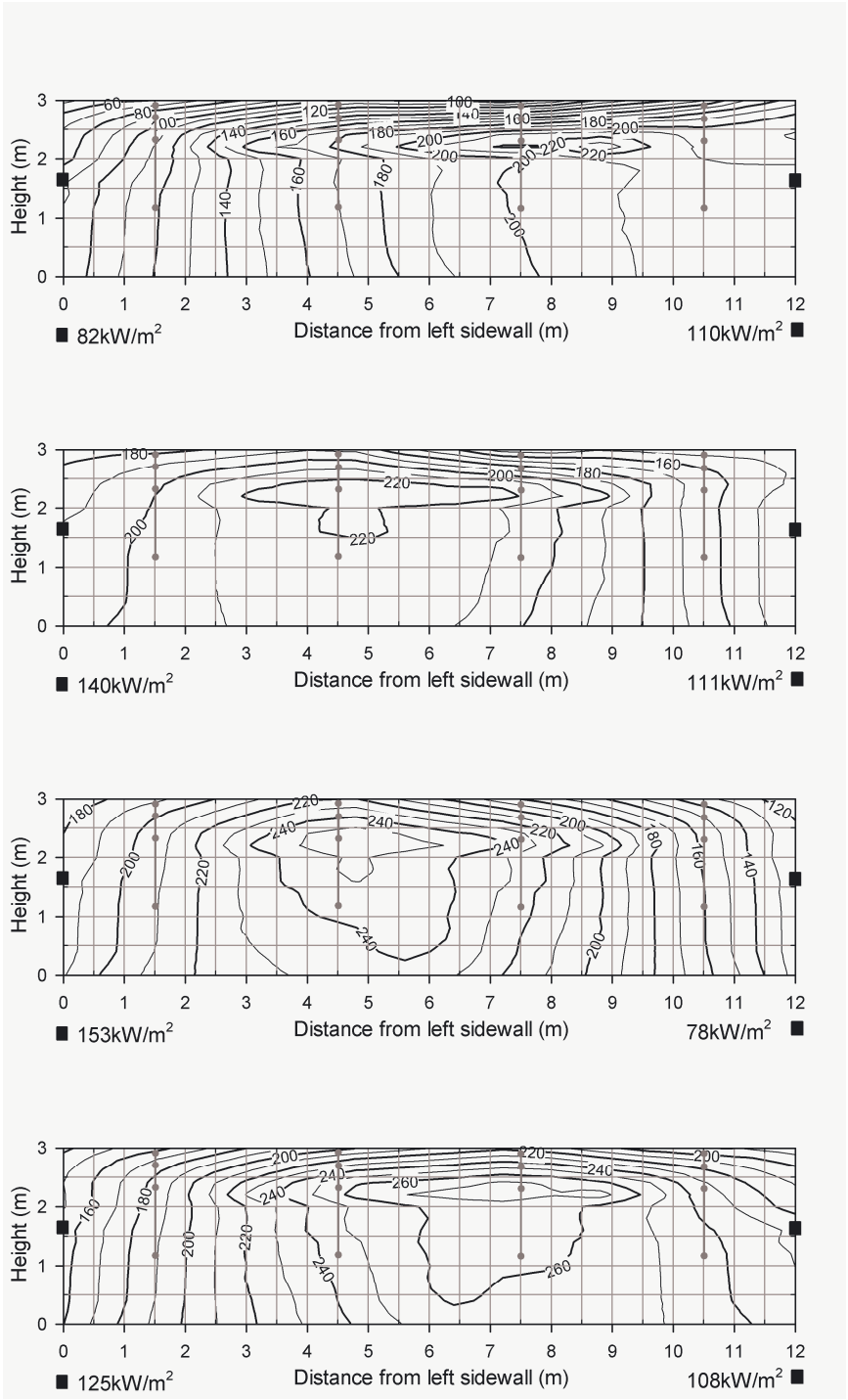

Fig. 14. Heat flux map over cross-section through centre of compartment (line 2, Figs. 1-2), viewed from front (test 8); bold numbers at sides indicate readings from billets 7 and 8 at positions of the black squares; contour labels in kW/m^2.

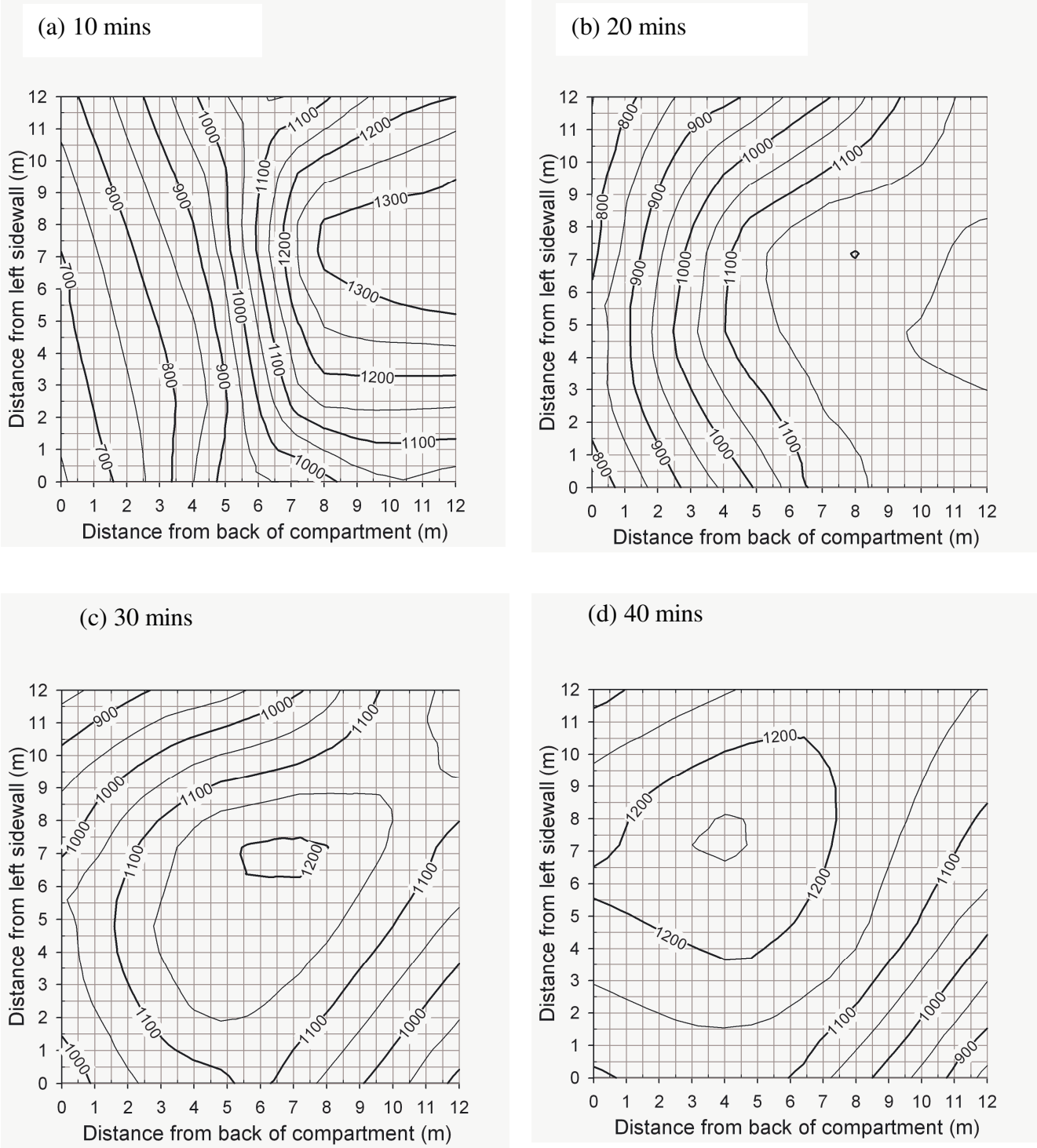

Fig. 15. Gas temperature map just under compartment ceiling (test 8); openings are located on right of each plot; contour labels in °C.

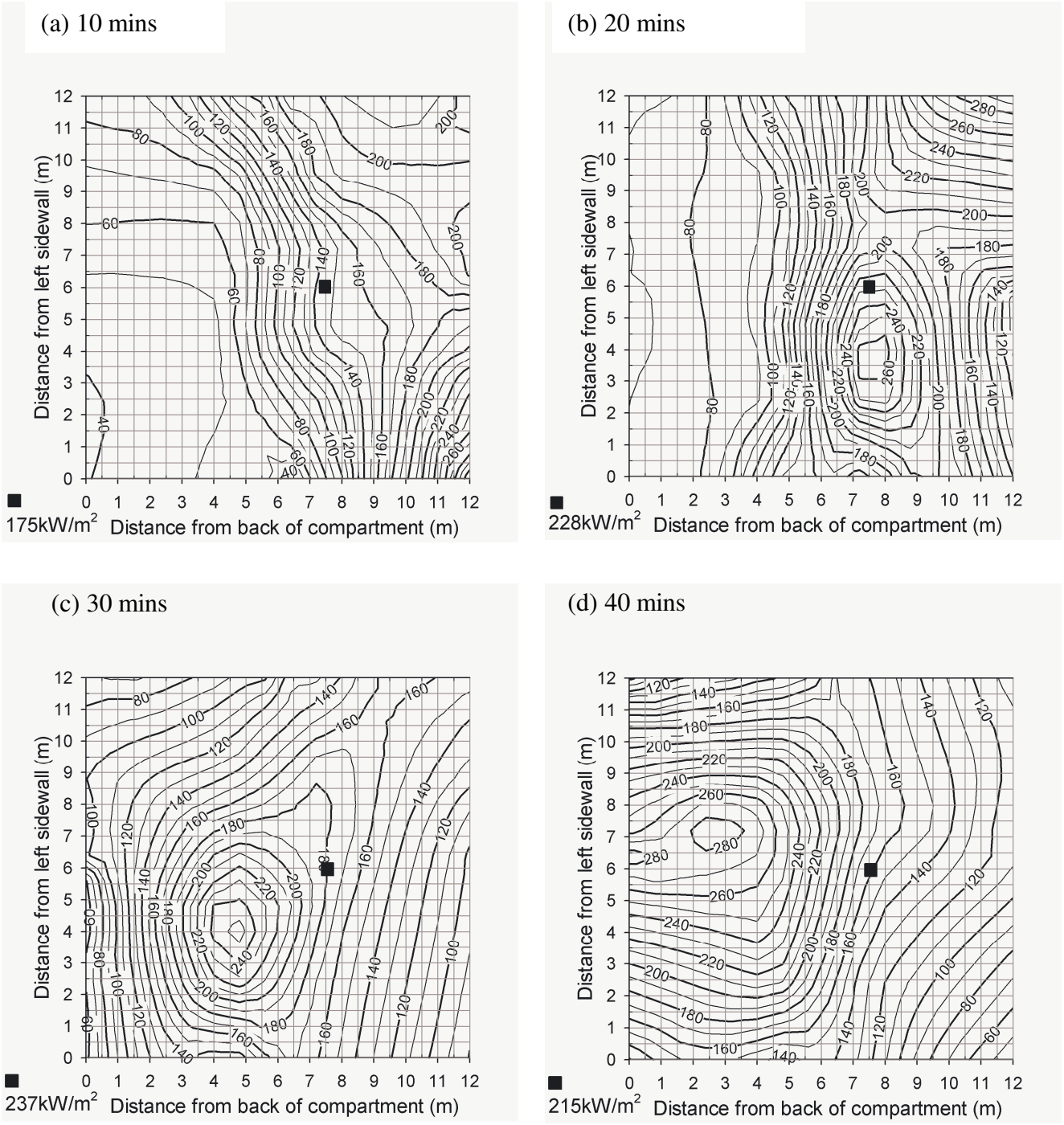

Fig. 16. Heat flux map just under compartment ceiling (test 8); bold numbers below plots indicate reading from billet 5 at position of the black square; openings are located on right of each plot; contour labels in kW/m^2.

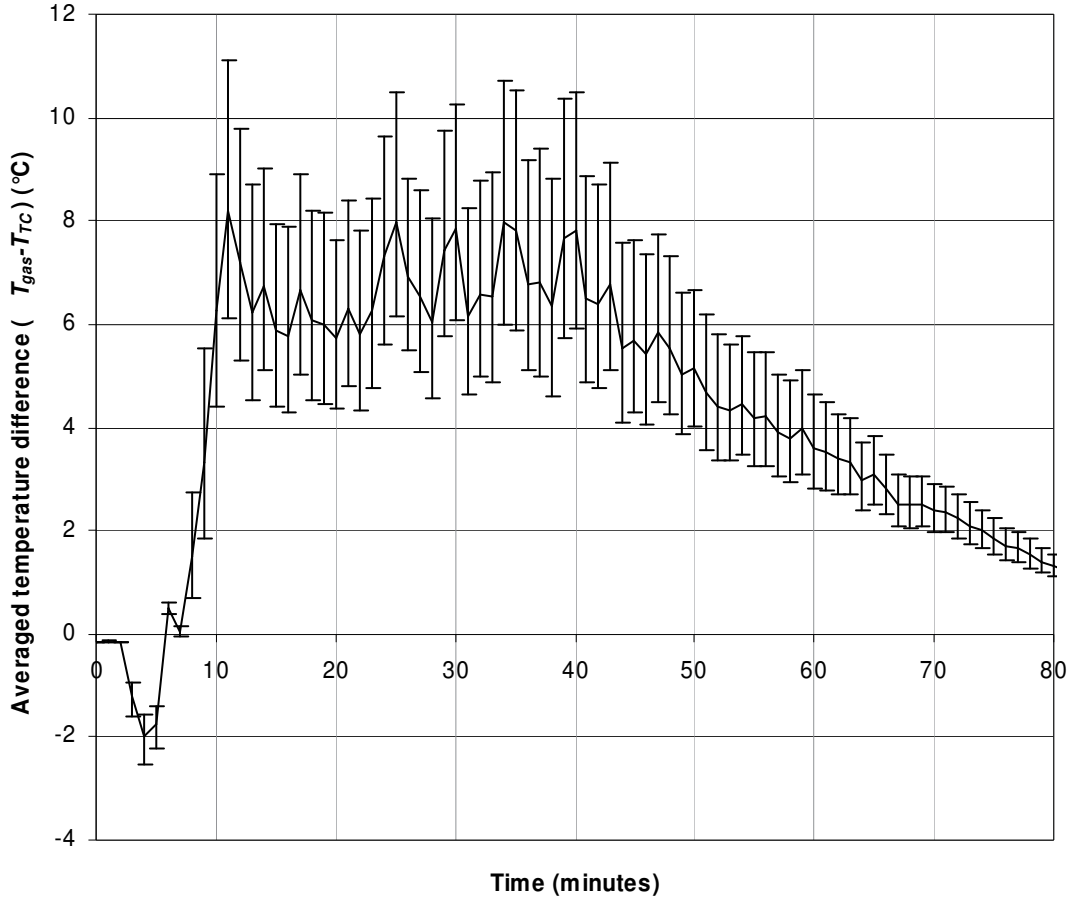

Fig. 17. Temperature differences, ($T_{gas} - T_{TC}$), averaged over all internal thermocouple locations (G1-G16/1-4) (test 8); error bars indicate extinction coefficient bounds (κ=0.8 and 1.2).